NAVAL POSTGRADUATE SCHOOL
Monterey, California

DTIC

THESIS

Acoustic Modeling of the Monterey Bay
Tomography Experiment

by

Lieutenant(N) Donald Fraser Smith

December 1990

Thesis Advisor:	James H. Miller
Co-advisor:	Ching-Sang Chiu

91-14255

Unclassified
Security Classification of this page

REPORT DOCUMENTATION PAGE

1a Report Security Classification Unclassified		1b Restrictive Markings			
2a Security Classification Authority		3 Distribution Availability of Report			
2b Declassification/Downgrading Schedule		Approved for public release; distribution is unlimited			
4 Performing Organization Report Number(s)		5 Monitoring Organization Report Number(s)			
6a Name of Performing Organization Naval Postgraduate School	6b Office Symbol (If Applicable) EC/Mr	7a Name of Monitoring Organization Naval Postgraduate School			
6c Address (city, state, and ZIP code) Monterey, CA 93943-5000		7b Address (city, state, and ZIP code) Monterey, CA 93943-5000			
8a Name of Funding/Sponsoring Organization	8b Office Symbol (If Applicable)	9 Procurement Instrument Identification Number			
8c Address (city, state, and ZIP code)		10 Source of Funding Numbers			
		Program Element Number	Project No	Task No	Work Unit Accession No

11 Title (Include Security Classification) ACOUSTIC MODELING OF THE MONTEREY BAY TOMOGRAPHY EXPERIMENT

12 Personal Author(s) Smith, Donald F.

13a Type of Report Master's Thesis	13b Time Covered From To	14 Date of Report (year, month,day) December 1990	15 Page Count 67

16 Supplementary Notation The views expressed in this thesis are those of the author and do not reflect the official policy or position of the Department of Defense or the U.S. Government.

17 Cosati Codes			18 Subject Terms (continue on reverse if necessary and identify by block number)
Field	Group	Subgroup	Acoustic Tomography, Acoustic modeling, eigenrays, Monterey Bay

19 Abstract (continue on reverse if necessary and identify by block number)
    In December 1988, a tomographic signal transmission test was conducted in order to test the feasibility of tomographic analysis in a region of complex bathymetry. The transmission test was conducted in the Monterey Bay where the signals propagated from deep water to shallow continental shelf water. In order to utilize the inverse techniques to infer the ocean processes affecting the acoustic propagation, the propagation paths of the tomographic signal between the transmitter and receivers must be determined. This thesis demonstrates that the forward problem of arrival path identification in the complex propagation environment of the Monterey Bay can be solved by using high resolution bottom bathymetry along with an appropriate sound speed profile as input to a three-dimensional Hamiltonian raytracing program, HARPO. The eigenrays found using this technique matched the travel times and relative amplitudes of the measured multipath arrivals.

20 Distribution/Availability of Abstract [X] unclassified/unlimited ☐ same as report ☐ DTIC users	21 Abstract Security Classification Unclassified	
22a Name of Responsible Individual James H. Miller	22b Telephone (Include Area code) (408) 646-2384	22c Office Symbol EC/Mr

DD FORM 1473, JUN 86   *Previous editions are obselete.*   SECURITY CLASSIFICATION OF THIS PAGE
                              S/N 0102-LF-014-6603   Unclassified

Acoustic Modeling of the Monterey Bay Tomography Experiment

by

Donald Fraser Smith
Lieutenant(N), Canadian Armed Forces
B.Eng.(E.E.), Royal Military College of Canada, 1983

Submitted in partial fulfillment of the requirements
for the degree of

MASTER OF SCIENCE IN ENGINEERING ACOUSTICS

from the

NAVAL POSTGRADUATE SCHOOL
December 1990

Author: _____
Donald Fraser Smith

Approved by: _____
James H. Miller, Thesis Advisor

_____
Ching-Sang Chiu, Thesis Co-Advisor

_____
Anthony A. Atchley, Engineering Acoustics
Academic Committee

ABSTRACT

In December 1988, a tomographic signal transmission test was conducted in order to test the feasibility of tomographic analysis in a region of complex bathymetry. The transmission test was conducted in the Monterey Bay where the signals propagated from deep water to shallow, continental shelf water. In order to utilize the inverse techniques to infer the ocean processes affecting the acoustic propagation, the propagation paths of the tomographic signal between the transmitter and receivers must be determined. This thesis demonstrates that the forward problem of arrival path identification in the complex propagation environment of the Monterey Bay can be solved by using high resolution bottom bathymetry along with an appropriate sound speed profile as input to a three-dimensional Hamiltonian raytracing program, HARPO. The eigenrays found using this technique matched the travel times and relative amplitudes of the measured multipath arrivals.

iii

TABLE OF CONTENTS

I. INTRODUCTION

Ocean acoustic tomography is used to determine dynamic processes in the ocean by measuring travel time perturbations of signal arrivals. The basis for the effectiveness of any tomographic analysis is the capability to reliably identify the paths that the acoustic energy propagates along through the ocean and to match the paths to the measured signal arrivals - this is called the forward problem.

In December 1988, a tomography experiment was conducted in Monterey Bay, the Monterey Bay Tomography Experiment (MBTE), which was designed to explore the feasibility of tomography in a region of complex bathymetry. The experiment encompassed diverse propagation regimes that included deep ocean water, the Monterey Submarine Canyon, the steep local continental slope and the shallow continental shelf. The depth regimes ranged from 90 to 2600 meters.

Tomography uses perturbations of the arrival times of the acoustic signals travelling along known ray multipaths. The perturbations in arrival time are converted into estimates of oceanographic parameters using inverse techniques. The rays that connect a particular source location to a particular receiver location are termed eigenrays. These eigenrays must be determined before inversion can take place.

The aim of this thesis was to incorporate a high resolution three-dimensional bathymetry and measured sound speed profiles into a fully three-dimensional propagation model to determine the eigenrays for one of the transmitter/receiver pairs. Also, the reliability of the modeled eigenrays was determined by perturbing the environmental inputs to match phenomena seen during the

1

experiment (i.e. depth changes due to tides and changes in the surface sound speed profile due to a local storm) and testing the sensitivity of the eigenrays to these changes. In order to model the Monterey Bay transmissions it will be shown that a three dimensional acoustic model is required. The model employed was developed at the Wave Propagation Laboratory of the National Oceanic and Atmospheric Administration and is called *Hamiltonian Acoustic Raytracing Program for the Ocean* (HARPO). This model has been modified at the Woods Hole Oceanographic Institution to allow user defined non-closed-form bathymetry and sound fields.

HARPO was utilized to determine the eigenray paths and travel times and to provide the required information to determine the transmission loss. The existing eigenray-finding routines were found to be inadequate due to the sensitivity of raypaths to the bathymetry. The technique developed to determine eigenrays in this thesis will be discussed.

It was found that the propagation paths could be successfully modeled and that the modeled arrival times compared well with the measured signal arrivals from the Monterey Bay Tomography Experiment. This led to a reliable identification of the propagation paths taken by the measured arrivals and successfully completed the first requirement for application of inverse techniques for this experiment.

The outline for this thesis is as follows:

Chapter II contains background information on ocean acoustic tomography, Hamiltonian wave theory, HARPO and the MBTE.

Chapter III specifies the Monterey Bay model environment and modeled variations during the MBTE used in the eigenray sensitivity analysis.

Chapter IV details the ray shooting method used to find eigenrays for the MBTE and compares it to other techniques applied to less complex propagation environments, the propagation loss estimation technique, and the eigenray sensitivity analysis.

Chapter V discusses the model results and sensitivity analysis of the eigenray paths and travel times, and presents the thesis conclusions.

II. BACKGROUND

A. OCEAN ACOUSTIC TOMOGRAPHY

"Ocean acoustic tomography is a technique for observing the dynamic behavior of ocean processes by measuring the changes in travel time of acoustic signals transmitted over a number of paths". [Ref. 1] Of crucial importance for any tomographic analysis is an accurate knowledge of the acoustic paths that join the transmitter and receiver. These paths determine the spatial resolution and coverage of a tomographic system as the ray interacts with large-scale oceanographic features (i.e. the bottom, eddies, gyres) and smaller-scale phenomena (i.e. internal or surface waves) [Ref. 2].

Most tomography experiments are designed so that geometric acoustics (ray theory) can be used to approximate the propagation of sound. Two simplified eigenray paths (an eigenray path joins the transmitter to the receiver) are presented in Figure 2.1 where: S_i and S_{i+1} are the eigenray paths and ds is a differential distance along the path. Using the geometric acoustic approximation the travel time, τ_i, of the ith eigenray, S_i, is given by

$$\tau_i = \int_{S_i} \frac{ds}{c(x,y,z)} \tag{2.1}$$

where

$$c(x,y,z) = c_0(x,y,z) + \delta c(x,y,z), \tag{2.2}$$

c_o is the initial sound speed, and δc is the perturbation of the sound speed along

4

the ray path. Use of the binomial expansion leads to the approximate value of τ_i

$$\tau_i \approx \tau_{oi} + \delta\tau_i \qquad\qquad (2.3)$$

where

$$\tau_{oi} = \int_{S_i} \frac{ds}{c_0} \qquad\qquad (2.4)$$

and

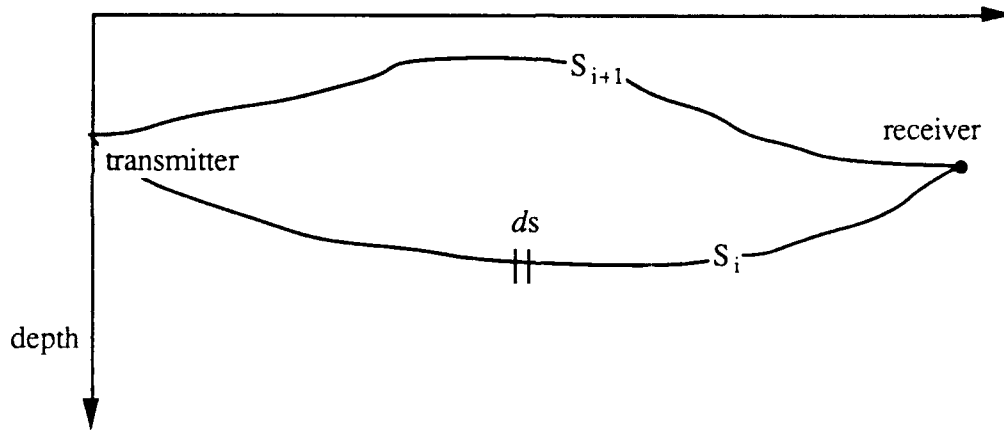$$\delta\tau_i = - \int_{S_i} \frac{\delta c}{c_0^2} ds \qquad\qquad (2.5)$$

Figure 2.1. Eigenray Path through an Inhomogeneous Medium.

In tomographic analysis τ_i is the measured travel time, τ_{oi} is the modeled travel time, and $\delta\tau_i$ is the measured difference. The measured difference is used, via inverse theory, to infer the large-scale ocean processes that effect the sound speed distribution along the propagation path. In order for the inverse

5

techniques to yield valid results the eigenray path, S_i, associated with each arrival time, τ_i, must be known.

B. HAMILTONIAN WAVE THEORY

B.1. Hamilton's Equations Applied to Acoustic Wave Propagation

An alternative to the traditional Snell's Law implementation of ray theory is to numerically integrate a differential form of Fermat's principle; in particular Hamilton's equations. The importance of this approach is that it involves a continuous model of the environment and the wave propagation through the environment. [Ref. 3]

Fermat's principle states that the raypath between any two points is the path for which travel time is a minimum; these are known as Fermat paths [Ref. 4]. Within the limits where ray theory approximates acoustic propagation, waves behave as particles which travel along rays in a manner analogous to changes of position and momentum in a mechanical system. The differential equations used to describe this system are Hamilton's equations of motion

$$\frac{\partial x_i}{\partial \tau} = \frac{\partial H_i}{\partial k_i} \; ; \; \frac{\partial k_i}{\partial \tau} = -\frac{\partial H_i}{\partial x_i} \; ; i = 1 \text{ to } 3 \tag{2.6}$$

where τ is a parameter proportional to time, the k_i's are the direction vectors, x_i are the co-ordinates of a point on the raypath, and H is the Hamiltonian function [Ref. 5].

The Hamiltonian function, H, describes the ray's total energy and is derived from the acoustic wave relation

$$H(x_i, k_j) = [\omega - \vec{k}_j \cdot \vec{V(x_i)}]^2 - c^2(x_i) k_j^2 = 0 \tag{2.7}$$

6

where ω is the angular frequency, $c(x_i)$ is the sound speed at x_i, and $V(x_i)$ is the ocean current [Ref. 3]. Equations 2.6 and 2.7 are for a three-dimensional rectilinear field and are implemented in spherical co-ordinates in HARPO.

The advantage of the Hamiltonian path-integral ray tracing technique is that it models a continuous ocean environment and raypath. The path integral method, as in HARPO, thereby avoids problems involving false caustics and discontinuities inherent in many models. These problems arise from applying closed-form solutions over discrete regions and then patching them together at cell boundaries. [Ref. 3]

B.2. An Overview of HARPO

HARPO is a general purpose, three-dimensional acoustic raytracing program which takes advantage of the Hamiltonian description of a raypath. By combining the initial conditions of propagation direction and position to a continuously described environmental model the Fermat path for each set of initial conditions is calculated. The calculated paths do not, however, account for diffraction or scattering by changes along the raypath smaller than a Fresnel zone.

The original version of HARPO has been modified to accept sound speed field and bathymetry entered on a evenly spaced grid; these are then smoothed with bi-cubic splines to provide the necessary first and second order derivatives needed to calculate the Hamiltonians. This feature requires that the input fields have continuous derivatives (first order for sound field, and first and second order for bathymetry).

As output HARPO generates "raysets" files for each Fermat path containing the required information (local wavenumber, ray travel time, geometric path

length co-ordinates) to identify eigenrays and to estimate transmission loss along the eigenray. Also because Hamilton's equations are being numerically integrated, HARPO allows for the trade-off of accuracy and computational speed by changes to the maximum integration error per step.

A detailed explanation of HARPO can be found in Reference 3; features of HARPO needed for understanding its implementation will be explained as necessary.

C. THE MONTEREY BAY TOMOGRAPHY EXPERIMENT

The Monterey Bay Tomographic Experiment had four goals:

1. Investigate experimentally the relation between the frequency-direction spectrum of surface waves and the spectra of travel time changes in tomography signals.

2. Investigate the effect of internal waves on tomography signals in a coastal environment.

3. Investigate the effect of complex three-dimensional bathymetry on long range propagation.

4. Test a real-time shore-based tomography data acquisition system. [Ref. 4]

The MBTE differed from prior tomographic experiments in that it was conducted in a coastal area with the transmitter/receiver raypaths crossing the continental shelf and Monterey Bay Canyon: most previous experiments having been conducted in open ocean locations with gradually varying bathymetry.

In general, the success of a tomographic experiment requires:

1. A stable set of eigenray arrivals to allow for reliable determination of travel time perturbations over long time periods,

2. Indentifiable eigenrays that correctly match measured arrivals times with the model raypaths.

8

3. Large enough temporal separation of eigenray arrivals to resolve individual rays (this depends upon array beamforming and transmitted signal bandwidth).

4. Signals that have sufficient signal to noise ratio to be detected with the chosen detection scheme. [Ref. 1]
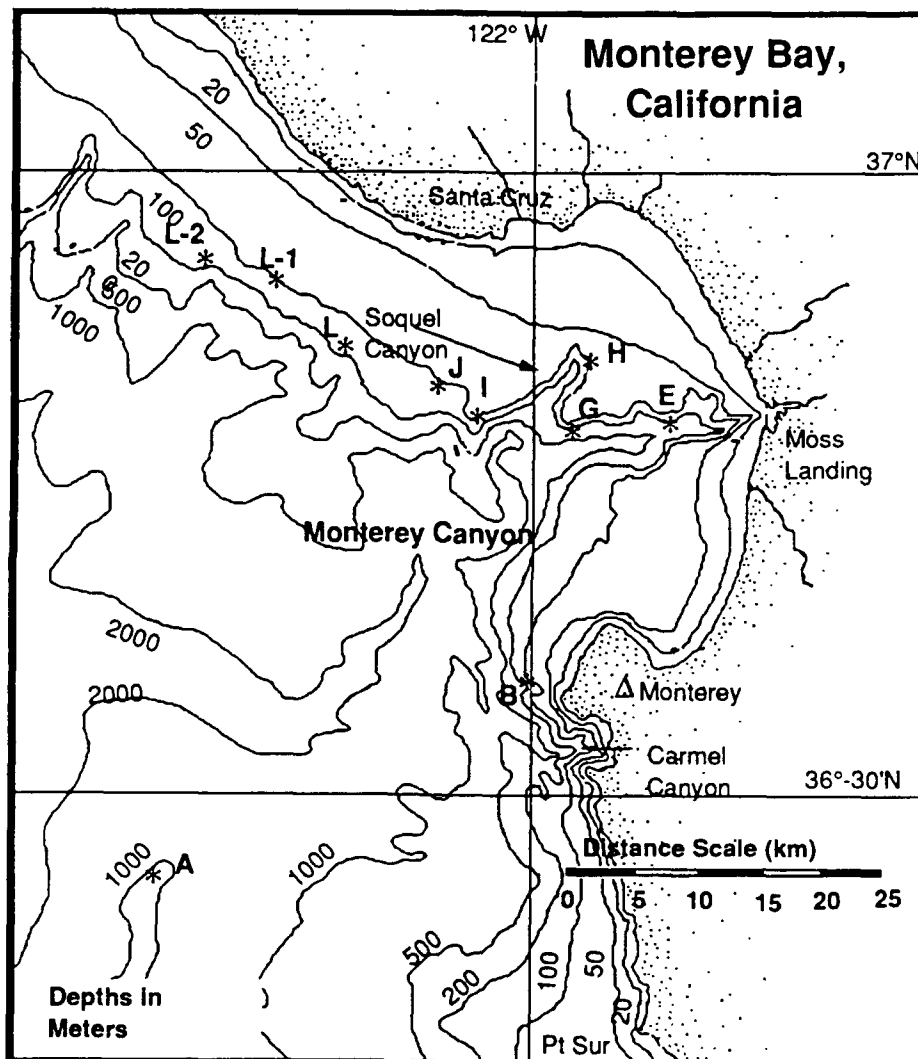
122° W **Monterey Bay, California**

37°N

Santa Cruz

L-2

L-1

Soquel Canyon

J I

H

G E

Moss Landing

Monterey Canyon

2000

2000

Monterey

Carmel Canyon 36°-30'N

Distance Scale (km)

0 5 10 15 20 25

1000 A 1000

500

200 100 50

Depths in Meters

Pt Sur

Figure 2.2. Location of Source (A) and Receivers (B - L-2) for the Monterey Bay Tomography Experiment.

In order to meet these requirements: the transmitter/receiver deployment points were optimized to exploit pre-deployment modeling using a two-dimensional model (MPP-Multiple Profile Ray Tracing Program); and the signal design was chosen to rapidly sample the desired spectra using the smallest possible signal bandwidth using the available source.

The locations of the source and receivers are given in Figure 2.2. The source, A, was deployed at 36° 23.7' N, 122° 17.84' N on the east side of an unnamed seamount off of Point Lobos. The receivers, B through L-2, were deployed on the sea floor in shallow water (100 meters) along the periphery of the Monterey Submarine Canyon. This geometry was predicted to provide acoustic sampling of both the deep water of the canyon and the shallow shelf water. In particular the predicted multiple bottom bounces in the shelf water would allow for each ray to "sample" the sea surface and any internal waves present on the shelf numerous times [Ref. 6]. The locations of the deployment sites were chosen based upon model results that indicated: that paths of predicted eigenrays passed through the bodies of water of interest; and that several identifiable and resolvable arrivals would be present to provide sufficient information for tomographic inversions.

The transmitter was secured within one meter of the sea floor in order to minimize movement due to ocean currents. It was a high-Q omni-directional resonant system. The transmitted signal was a m-sequence phase-modulated signal with a center frequency of 224 Hz. When demodulated to baseband the signal decodes into a pulse train of 62.5 msec wide pulses repeated every 1.9375 seconds (Figure 2.3).
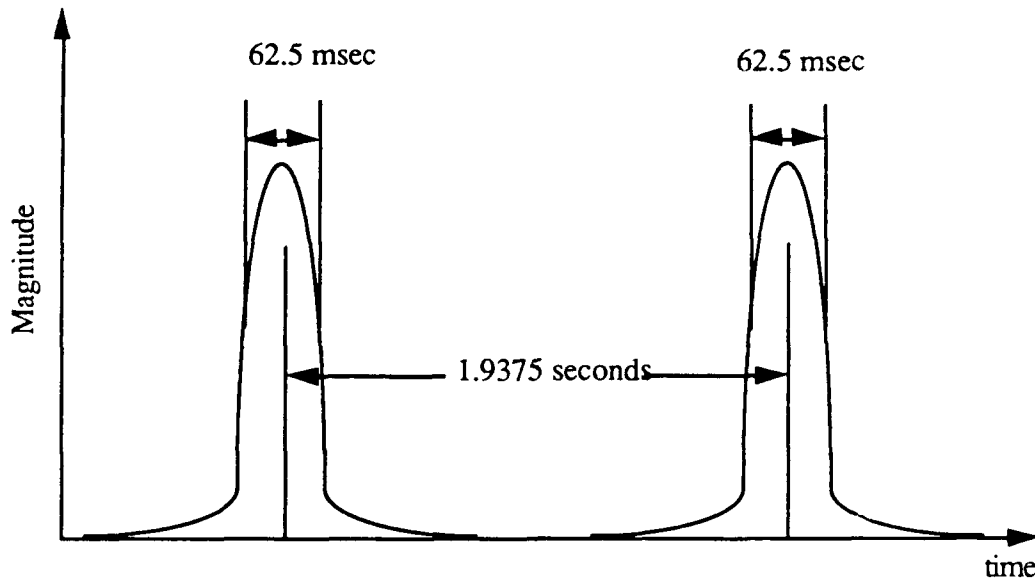
Figure 2.3. Magnitude of Transmitted Signal after Demodulation and m-Sequence Removal.

This signal design has several implications. First, predicted eigenray travel times were in the order of 35 to 40 seconds. Since the receiver was not time synchronized with the transmitter and the pulse repitition rate was less than the predicted eigenray travel time, absolute travel times could not be measured. The only available arrival time results were arrival time differences that were repetitive over the pulse repition rate of 1.9375 seconds. The best technique for matching the signal arrival versus time to predicted eigenray plots is to order the predicted eigenray arrival times and 'slide' the predicted arrivals over the measured arrivals to find the best pattern fit (this technique will be more fully discussed in Chapter 4). Secondly, with a pulse width of 62.5 msec, any arrivals with arrival time differences of less than this pulse width will be unresolvable to the receiver system. This means that arrival times of these closely spaced rays would not be measurable as illustrated in Figure 2.4(b).

11

Finally, any detectable arrival with a difference in travel time of more than 1.9375 seconds from the reference eigenray will cause an ambiguity in travel time. This means that two signals with arrival times that differ by an integral number of sequence lengths, i.e. τ_i and τ_i - n*(1.9375) seconds where n is any integer, are indistinguishable with this signal scheme because total travel times are unknown. Figure 2.5 illustrates this phenomenon with an example where n=1.
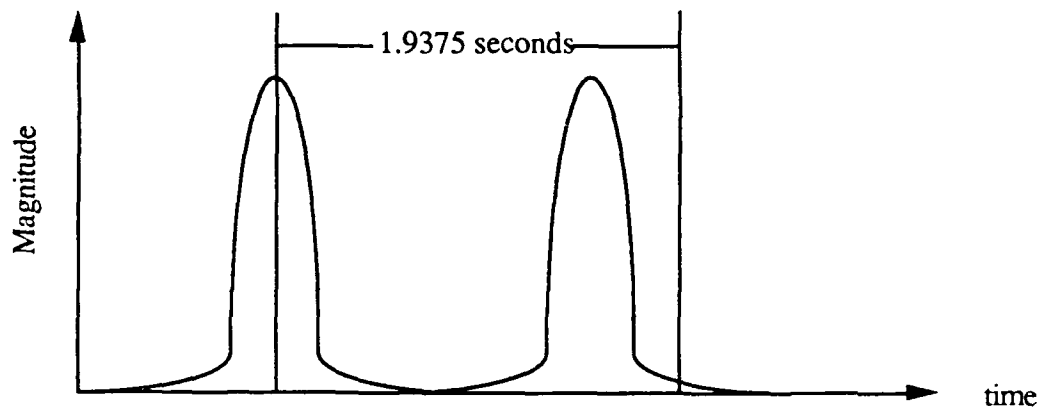

Figure 2.4(a). Two Resolvable, Unambiguous Signal Arrivals.
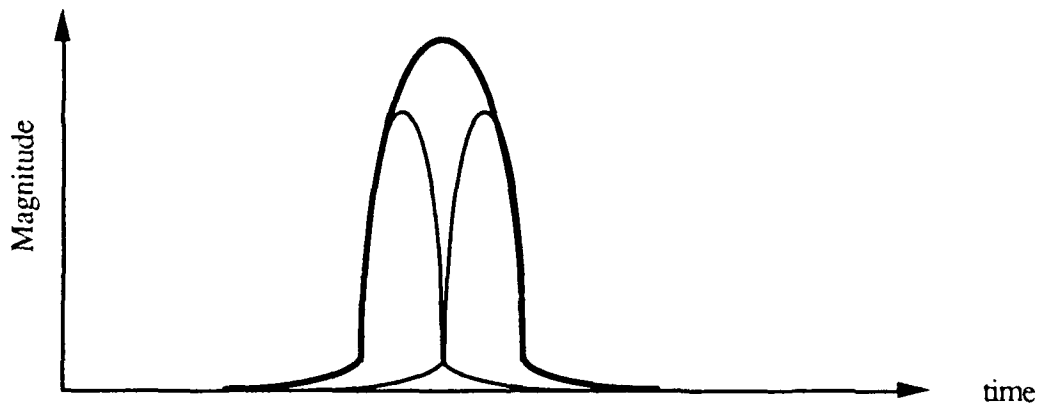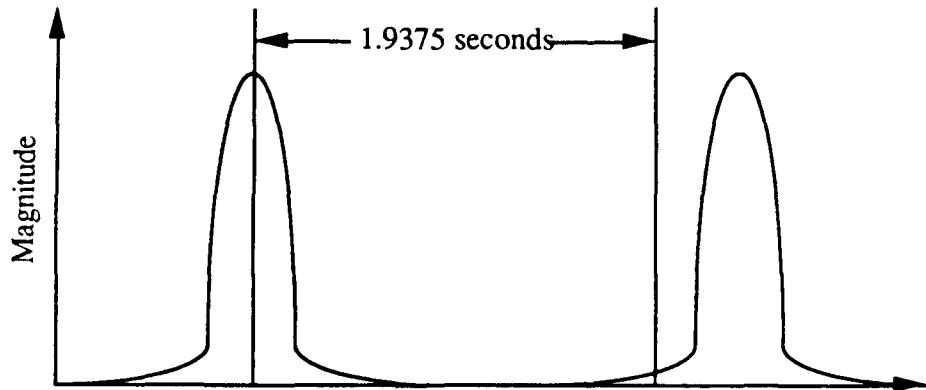

Figure 2.4(b). Two Unresolvable Signal Arrivals.

Figure 2.5. Two Resolvable Signals with an Ambiguity in Time Equal to One Sequence Length.

As will be shown, the data indicates that the signal and transmitter/receiver geometry was successfully designed. However, predicted (using MPP, a two-dimensional raytracing program) and measured arrival times differed substantially. The determination of the eigenrays using HARPO, a three-dimensional raytracing program, for the deployed system is the goal of this thesis.

III. MODELING THE MONTEREY BAY

A. INTRODUCTION

In order to determine the acoustic propagation in Monterey Bay an accurate
environmental model was incorporated into HARPO. The accuracy required is
determined by the acoustic properties of the medium and the expected
interactions at boundaries (sea-surface and ocean bottom). In particular the
bathymetry (both in absolute depths and bottom gradients) and the gradient of
the sound speed profile need to be known accurately to correctly determine the
eigenrays using any propagation model. However, the bathymetry and sound
speed profiles are sparsely sampled in most experiments, the MBTE being no
exception, and the modeler is left to most effectively meld the available data to
the model.

This chapter describes the environmental modeling required to predict the
eigenray paths from the transmitter to Station J. Particular emphasis is given to
the bottom bathymetry as it was expected to act as the largest factor in
determining which rays could reach the receiver. The characterization of the
sound speed field is also discussed as well as a brief statement of the tidal
phenomenon and effects these phenomena had on eigenray identification and
stability.

Figure 3.1 shows the section of the Monterey Bay that defines the
geographical limits of the environment modeled as input for HARPO. Within
this region bathymetry, sound speed and tidal effects were modeled and for
raytraces that crossed out of this region the results were determined as invalid

14

launch angles for possible eigenrays. The range in latitude is from 36°20'N to 37°00'N and in longitude is from 122°00'W to 122°20'W.
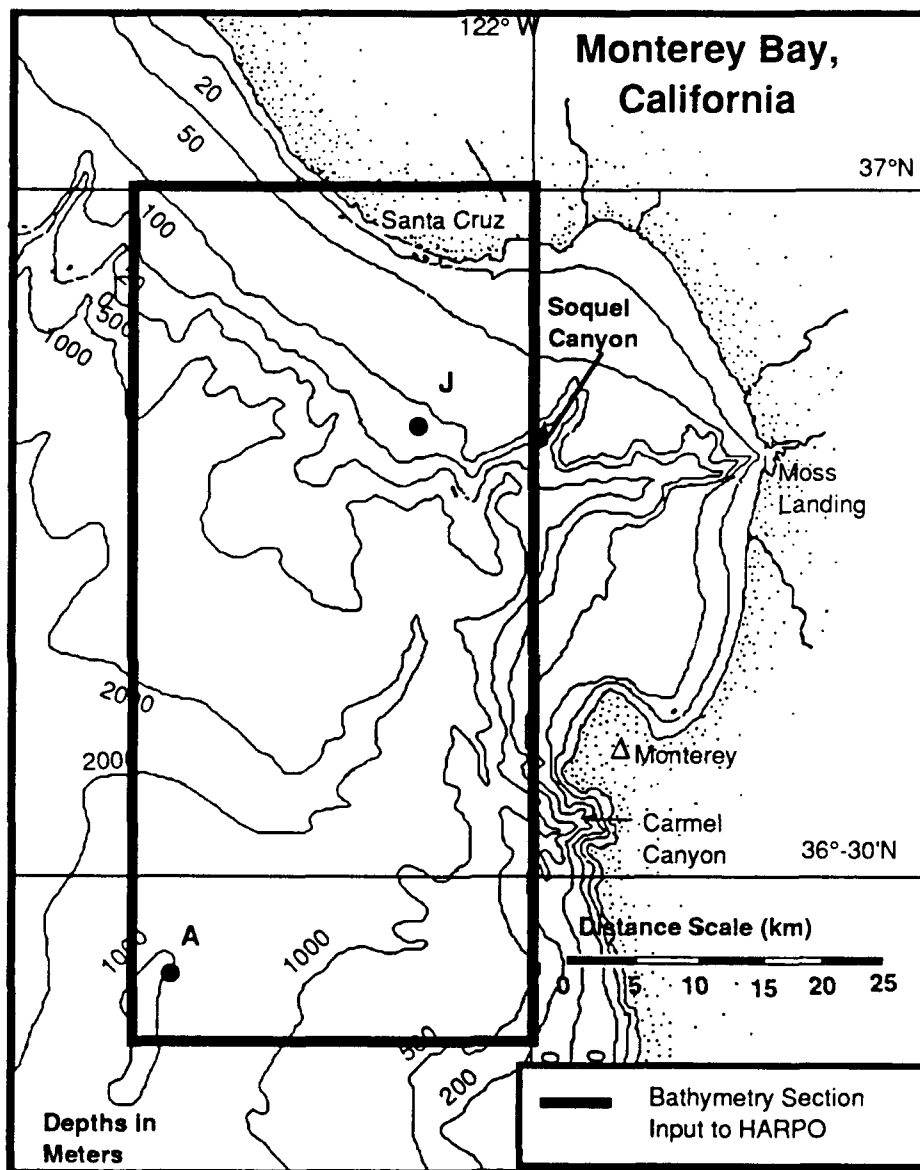

Figure 3.1. **The Geographical Boundaries for the HARPO Environment Input Model.**

B. MONTEREY BAY BATHYMETRY

The line-of-sight path joining the transmitter and station J traverses a rugged bathymetry and various bottom types. The dominant features are the unnamed seamount upon which the transmitter was deployed, the Monterey Submarine Canyon (MSC), one of the MSC's tributaries - the Soquel Submarine Canyon, and the narrow section of the continental shelf north of the MSC where receiver J was deployed (referred to as Station J). Figure 3.2(a) is the bathymetry for the section of the Monterey Bay used as input into HARPO (refer to Figure 3.1) and Figure 3.2(b) is the depth contours in meters for this section of bathymetry.

The transmitter was deployed on an unnamed seamount at $36^{\circ}23.7'N$ $122^{\circ}17.8'W$ in a depth of 850 meters. The transmitter was located 50 meters below the average deep sound speed minima at 800 meters; the average sound speed axis was determined from conductivity, temperature, depth (CTD) measurements made near the transmitter (see section C). [Ref. 2]

North of the transmitter is the Monterey Submarine Canyon, the largest submarine canyon on the California coastline. It has a volume of 470 km^3 and depths ranging from 18 meters at its origin off Moss Landing to 2925 meters at its junction 94.5 kilometers westward with the Monterey Fan Valley. For the line-of-sight from transmitter to station J the MSC provides the deepest bathymetry at 2600 meters depth. [Ref. 6]

Separating the MSC from the Soquel Submarine Canyon along the line-of-sight is a south-eastwardly sloping fan-like feature which has depths from 800 to 1500 meters and with which all the eigenrays had bottom interactions. The slope can be seen to have irregular folds in its shape and these were significant in determining eignrays.
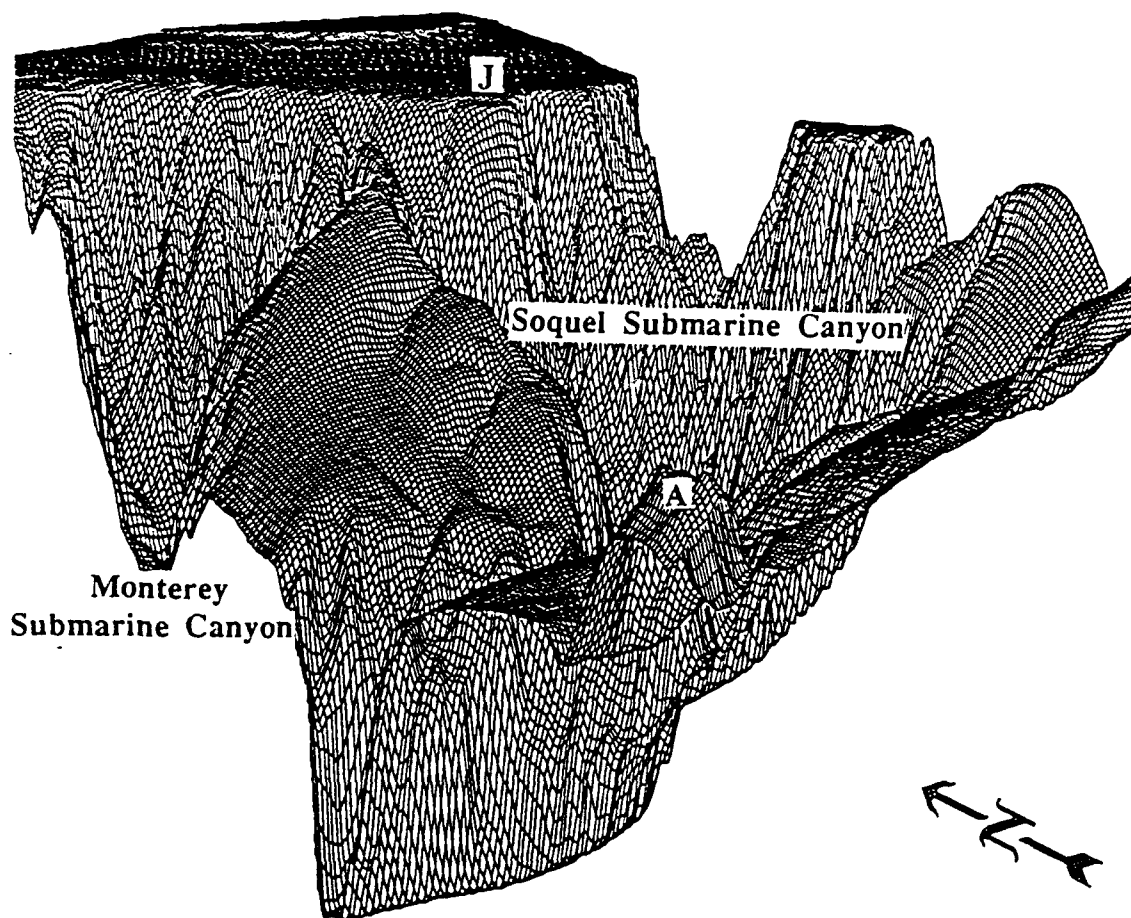
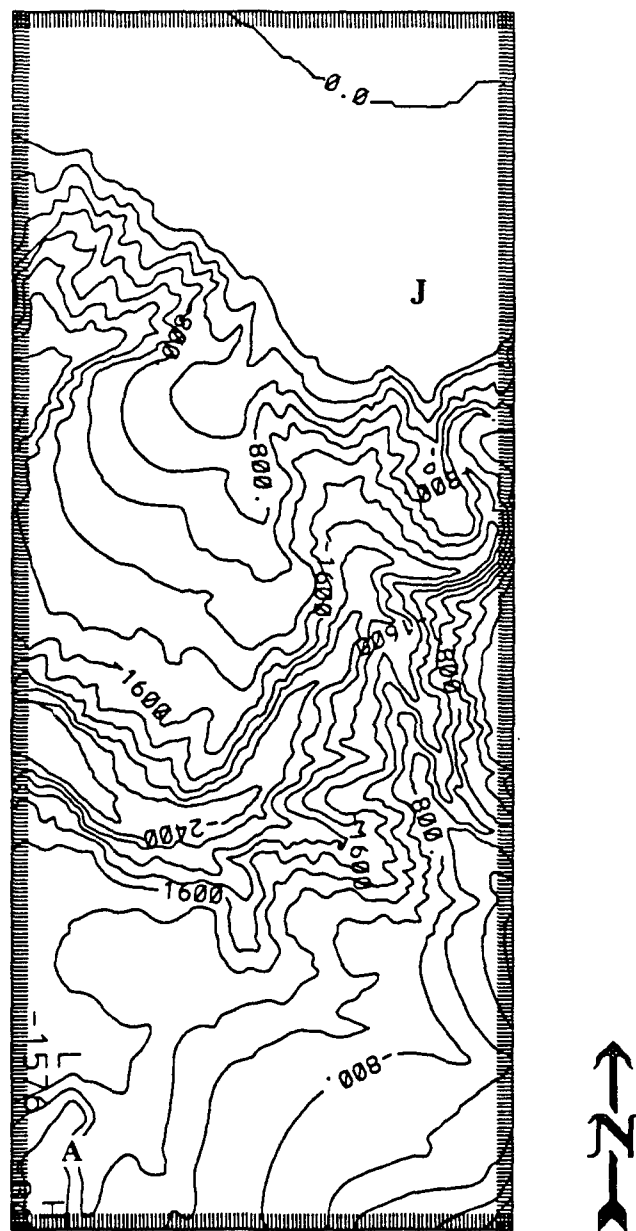Figure 3.2(a). Section of Monterey Bay Bathymetry Used to Determine Eigenrays at Station J.

Figure 3.2(b). Depth Contours of the Section of Monterey Bay
Used to Determine Eigenrays at Station J.

The Soquel Submarine Canyon was the next feature traversed by all eigenrays. Its very steep northern slope proved to be the most significant environmental feature that limited acoustic energy from propagating onto the continental shelf.

The bathymetric data used were provided by the Ocean Mapping Section of the National Oceanic and Atmospheric Administration and were extracted from two Economic Exclusion Zone data sets - LM137 N365121W/N365122W (Monterey Canyon) and LM 139 N360122W (Shepard Meander). The majority of the data was collected between 1985 and 1988 by the NOAA Bathymetric Swath Sounding System (BSSS) and the Sea Beam multibeam swath sound ship. Data in depths exceeding 600 meters were collected by the Sea Beam system, intermediate data from 150 to 600 meters were collected by the BSSS and the shallow water data were obtained from earlier standard NOAA hydrographic surveys. [Ref. 7]

The bathymetric data were provided with a resolution of 250 meters and were projected on to a Universal Transverse Mercator (UTM) grid based upon the NAD83 Spheroid. The soundings had been corrected for the in situ speed of sound and were given for low tide conditions. [Ref. 7]

In order to be used as input to HARPO the UTM co-ordinates were converted to spherical co-ordinates for the section of bathymetry required. The conversion gave a maximum spatial error of five meters at the northern corners of the grid; this was much less than the 250 meter grid resolution. After the co-ordinate conversion the grid was input to a bi-cubic spline subroutine that provided the necessary continuous bottom derivatives needed in HARPO without smoothing the bathymetry.

19

Figure 3.3 shows a section of the Monterey Bay bottom types. From this figure it is evident that any eigenray with bottom interactions would sample a variety of bottom types. However, it was not within the scope of this thesis to make the necessary changes to HARPO to handle the two major bottom modeling criteria - the sediment depth and the bottom sublayer structure. Therefore all eigenray calculations were for rigid bottom reflections and the method to quantify bottom loss in the propagation loss calculations will be discussed in Chapter Four.

LEGEND

COARSE AND MEDIUM SAND

FINE SAND

VERY FINE SAND

SILT AND CLAY

ROCK AND GRAVEL WITH SAND

COARSE SEDIMENT OVERLIES SILT AND CLAY

GRANODIORITE OUTCROPS WITH SAND BOTTOM

SHALE

SHELL GRAVEL

SANTA CRUZ

MOSS LANDING

MONTEREY

NAUTICAL MILES
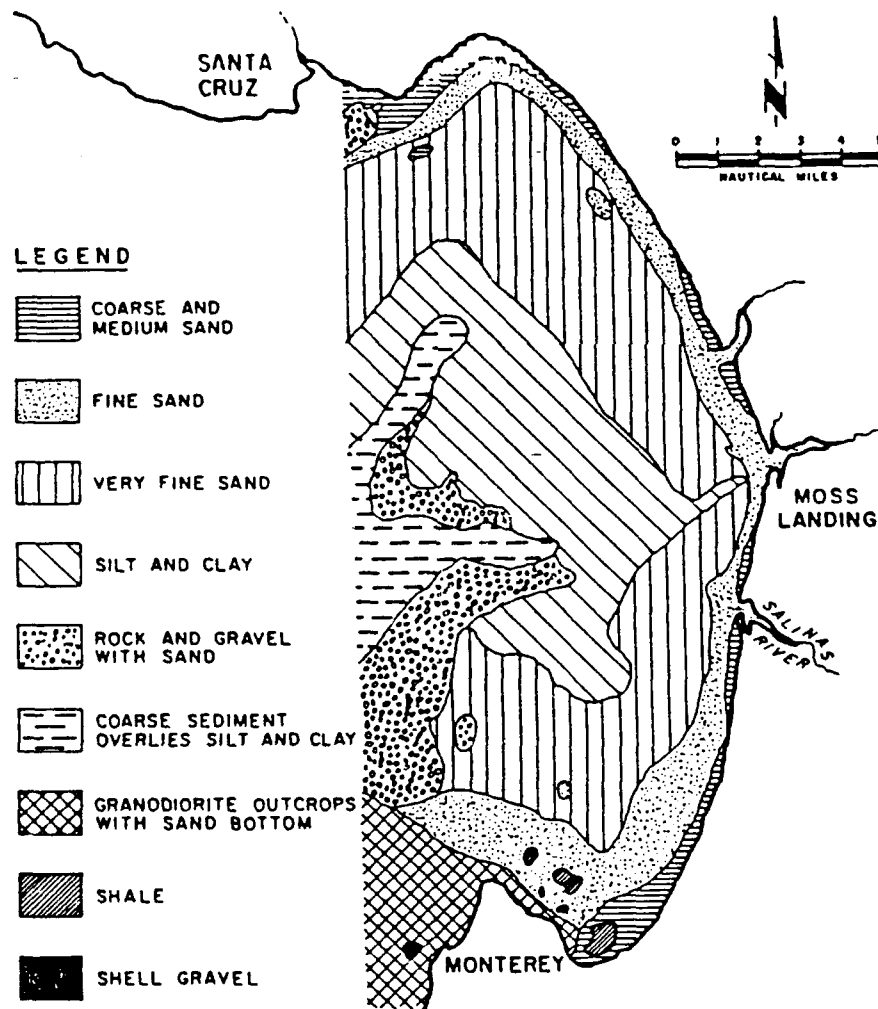
Figure 3.3. Bottom Types in Monterey Bay [Ref. 6].

C. SOUND SPEED STRUCTURE

Although the bottom reflections from the rugged bathymetry provided the largest effect upon the raypaths calculated by HARPO, the vertical gradient of the sound speed field was the major effect upon acoustic propagation direction between these bottom interactions. From CTD (conductivity, temperature and depth) measurements made at various locations throughout the experiment the speed of sound as a function of depth was calculated.

There were three measurements taken in the region of expected eigenray propagation for the transmitter and station J path. Two of these were taken on the shelf near station J two days apart and the third was taken in deep water between the transmitter and receivers.
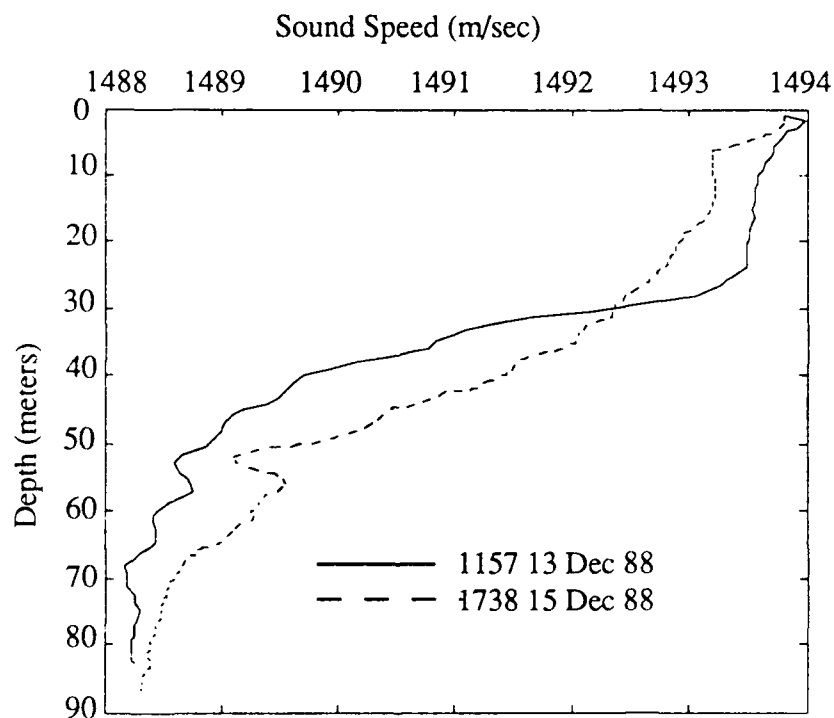
Figure 3.4. Sound Speed Profiles for Station J.

Figure 3.4 shows the results from the CTD measurements near Station J. The first was sampled at 36°51.0'N 122°04.8'W at 1157 13 December 1988. The second was sampled at 36°52.8'N 122°10.7'W at 1738 15 December 1988. In both cases the measurements were made in a vertical yo-yo fashion to determine if there were any changes in layer depths due to internal waves. For the purposes of modeling the vertical runs were averaged to give a mean sound speed over the measurement period.

It can be seen in Figure 3.4 that the strong mixed layer at 30 meters was not evident two days later at a different location (approximately 10 kilometers away and within 1.5 kilometers of the edge of the continental slope). This combination of 10 kilometer separation and proximity to the continental slope indicates that the two CTD's were likely measuring different water masses (see the section on currents in the Monterey Bay). The modeling of eigenrays used the 13 December profile as the baseline shallow water profile and the 15 December profile for the sensitivity analysis.

To model the deep water section of the Monterey Bay the results of the measured CTD's were averaged together to produce a mean profile for depths greater than measurements at station J. This was added to the representative near-surface sound speed profiles at station J so that eigenrays could be found and their character compared for the different profiles. The decision to use a single sound speed profile for the complete Bay was predicated by the closeness of the measured sound speeds, the lack of sufficient measurements along the line-of-sight to warrant a range dependent sound speed field, and the intuition that the bottom bathymetry would have a more severe effect on eigenrays in the deep

water sections (raypaths that had yet to reach the shelf) than the near surface errors in sound speed gradient introduced by this technique.

In order to implement the chosen sound speed profiles with HARPO it is necessary to provide a smooth analytical function of sound speed versus depth so that the gradients can be determined at all depths without any discontinuities. This was done for the irregularly sampled (in depth) sound speed profile by using the HARPO subroutine - CTANH which joins linear segments of the sound speed profile with hyperbolic functions. HARPO is only designed to allow 19 sound speed layers so the choice of layers was based on best modeling of the near-surface and near-axis segments of the measured profile. Figure 3.5 is the hyperbolic fitted sound speed profile used with the HARPO runs.
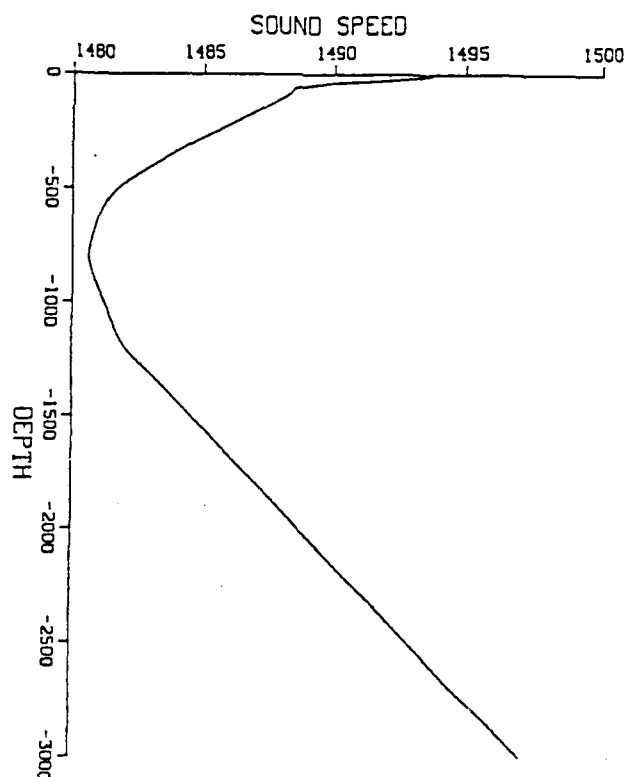
Figure 3.5. Sound Speed Profile Used by HARPO.

D. TIDES

The tides within the Monterey Bay are mixed semi-diurnal tides. Figure 3.6 shows the typical tidal pattern of two high tides and two low tides of different maximums and minimums that occur within Monterey Bay daily. The maximum difference in tidal extrema is approximately two meters and these extrema are measured throughout Monterey Bay in a 15 minute time span.
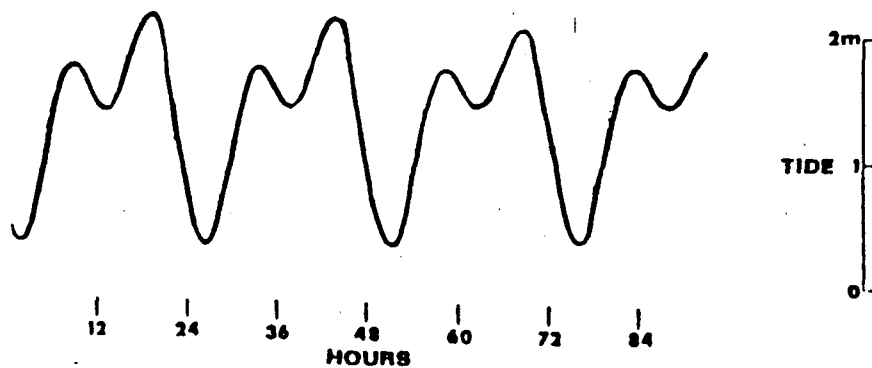

Figure 3.6. Monterey Bay Tidal Pattern.

For the purposes of modeling the eigenray sensitivity in the Monterey Bay the two meter tide was simulated by increasing the water depth by two meters. The sensitivity analysis will be discussed further in Chapter Four.

E. CURRENTS

Details of the Monterey Current flow are given in Reference 6. During the experiment the strongest ocean feature was the Davidson Current which is driven close to shore by wind and Coriolis forces. This nearshore current passes the Monterey Bay in a northerly direction as a large open eddy. Within Monterey Bay the currents during the winter circulate slowly and irregularly. Figure 3.7

shows typical current distribution when the Davidson Current is the driving factor.

Although acoustic Doppler current profiler data were collected during the experiment they were not incorporated into the HARPO model because the measurements were sufficiently off of the line-of-sight to make extrapolating their effects to the region of interest of questionable practicality.
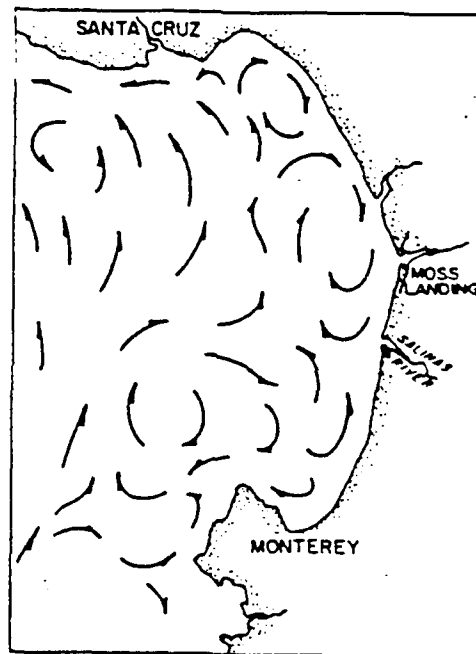

Figure 3.7. Monterey Bay Currents during the Davidson Current Season.

IV. EIGENRAY DETERMINATION

A. INTRODUCTION TO EIGENRAY SEARCH TECHNIQUES

In early tomography experiments the source/receiver geometries were designed so that the eigenray paths would be limited to the deep sound channel. This design greatly facilitated the determination of the eigenrays as there were no bottom interactions and the eigenray path deviations from the line-of-sight were assumed to be negligible.

One technique for determining eigenrays for azimuth independent propagation is to interpolate between rays shot over a range of elevation angles. For example, to model the tomographic array performance for the Greenland Sea Tomography Experiment, Kao [Ref. 8] used a linear sound speed profile. The eigenrays to be located were limited to rays without bottom interactions. The sound speed profile and raypaths for part of the launch angles used in the eigenray search are shown in Figure 4.1.
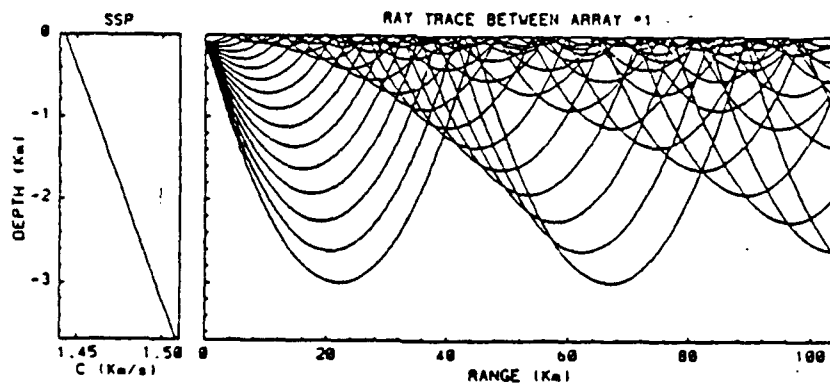

Figure 4.1. Typical Sound Speed Profile and Ray Paths used to Determine Eigenrays [Ref. 8].

The resulting ray depth at the receiver range is plotted versus the launch angle with a horizontal line at the receiver depth superimposed as shown in Figure 4.2. The points where the arrival depth curve intersects the receiver depth indicate the launch elevation angles of eigenrays.
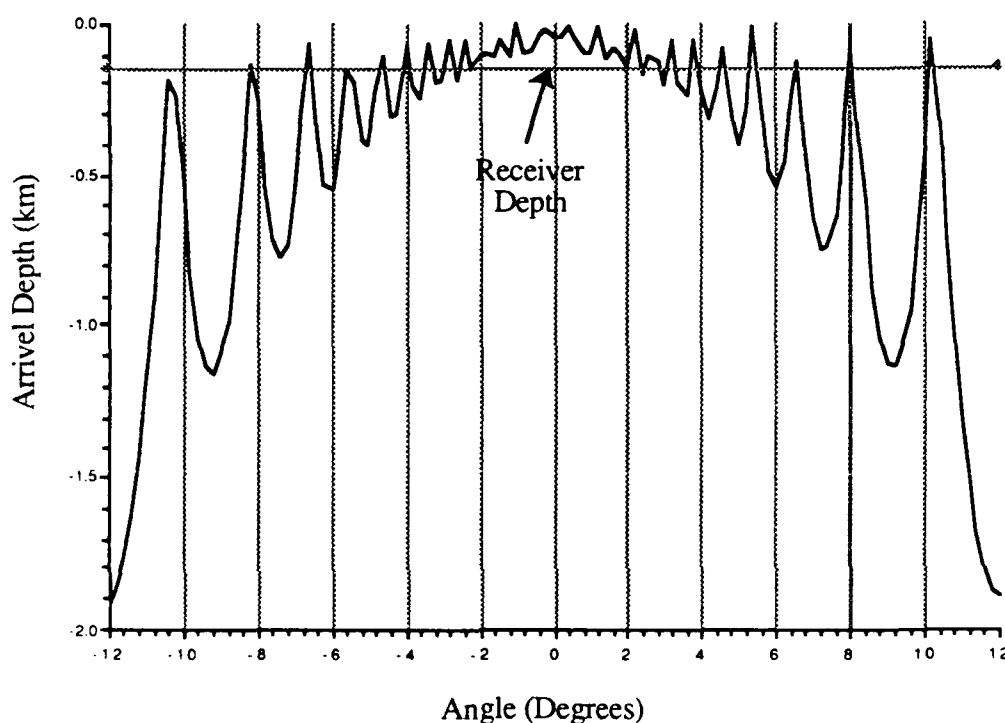

Figure 4.2. Arrival Depth Versus Launch Elevation Angle Used for Determining Eigenray Launch Angles.

This method requires, in addition to radially symmetrical propagation, that small changes in launch angle correspond to small changes of depth and ray angle at the the receiver range and that these changes are also smooth functions of the variation of launch angle.

Results from early tomography experiments indicated that the horizontal deflections of ray paths caused by mesoscale structures and current shears were

measurable and needed to be modeled. Mercer et al [Ref. 9] illustrates a method of using HARPO to find eigenrays for a gaussian-shaped mesoscale eddy. The key to the technique used was knowing the shape of the eddy and the effects the gradients in the horizontal sound speed field would have on the horizontal deflection of a ray. With this information it is possible to interpolate the correct azimuth launch angle of rays similar to the eigenray and then search in elevation to locate that particular eigenray. This technique also assumes that the ray paths change smoothly with changes in launch angles.

Both of these techniques are computationally efficient in that a sparse set of rays can be used to accurately interpolate the launch angles of the eigenrays and thereby save shooting many densely spaced rays to find these eigenrays.

B. SEARCHING FOR EIGENRAYS

It was found that both the two-dimensional arrival depth interpolation and azimuth interpolation for smoothly varying three-dimensional features methods were inappropriate for application to the Monterey Bay Tomography Experiment. The fundamental assumption in both techniques that a small launch angle perturbation results in a small ray path perturbation at the receiver was found to be invalidated when there was propagation interacting with rough bathymetry. This section describes the procedure used to locate eigenrays for the MBTE using HARPO.

The criteria chosen to determine eigenrays was any ray with a calculated raypoint that was within a half wavelength (3.35 meters at a frequency of 224 Hz) of the receiver was chosen as an eigenray. HARPO calculates points along the raypath (called a raypoint) that are determined when the maximum error for that integration step of the numerical integrator is reached. The choice of this

maximum error per integration step is a variable that controls the precision of the raypoints calculated as well as determines the computational run time for each ray calculation.

The nonlinear effect upon the raypath caused by the bathymetry meant that the previously described techniques employing interpolation techniques to reduce the computation of many rays were not employable. Indeed it was found that, although the ray paths were expected to vary smoothly in the very near vicinity to an eigenray, the combined effects of the bottom gradients and the numerical error accumulated along the raypath caused the rays to exhibit unsmooth changes even when launch angle changes as small as 10^{-5} degrees were used. An estimate of the numerical error accumulated was found by shooting rays spaced at 10^{-6} degrees. Also it was found that the corresponding raypoints at the receiver range differed by more than four meters and that raypoints for launch angles with intermediate values did not vary smoothly between these endpoints and differed slightly from run to run. The error expected for numerically integrating the Hamilton equations using an Adams-Moulton predictor-corrector method with a Runge-Kutta starter and a specified step error of 10^{-9} was on the order of 10^{-7} of the range [Ref.3]. This expected range error was less than the four meters computed. This large range error and the randomness of the intermediate raypoints indicated that the numerical precision of the calculations was being reached. It was found that the resident HARPO code had the double precision variables inconsistently implemented - this problem was only partly corrected in producing results presented in this thesis. However, the majority of eigenrays were found to have raypoints within the specified half wavelength hemisphere centered on the bottom mounted receiver position.

To optimize the use of HARPO in finding eigenrays the following subroutines and program modifications were implemented:

1. Subroutine RHORIZ was used. This subroutine generates a spherical surface at the specified depth and when any ray crosses this surface the ray characteristics are output to DOUTP (the user readable file of raypoints). The horizontal surface was set at the receiver depth at Station J (95 meters).

2. The maximum range for calculating raypaths was set at the transmitter/Station J range of 54.259 kilometers. This meant that all ray calculations were terminated when the ray's range exceeded 54.259 kilometers.

3. Any rays that left the boundaries of the modeled bathymetry were terminated.

4. Any rays that veered more than 90° from the previous azimuthal bearing were terminated.

5. Any rays that reversed direction (i.e. after reflection with a step surface) and propagated back towards the source were terminated.

6. Any rays that had a combination of more than 50 receiver depth crossings, surface reflections and bottom reflections were terminated. This limited the number of accepted bottom bounces to less than 16.

7. Any rays which failed to successfully back-up and find the bottom after bottom intersection were terminated. The criteria used was a difference of more than 3 meters between the actual and computed depths. This was a critical modification because there were a large number of rays (approximately 10 %) that did not pass this test. It was found that the bottom backup technique [Ref. 3] was chosen as it was the easiest to implement and had not been tested upon such rough bathymetry [Ref. 10]. This problem was overcome by increasing the integration error to 10^{-5} for these ray groups.

With these changes implemented the technique used to find the eigenrays was a straight forward shooting method. Rays spaced at 10^{-2} degrees in azimuth and elevation for an azimuth range of +/- 15° either side of the line-of-sight (20.481° east of north) and an elevation range of -10° to 75° were the initial search. For

any of these rays that missed the receiver by less than 500 meters a denser ray set of 10^{-3} degree increments was used. These rays were found to be in groups and denser searches were done as the miss distance was reduced to 100 and then 20 meters and finally rays that met the eigenray criteria. In not all cases did the search result in eigenrays being located. There were many cases where the rays would not converge beyond a certain point and this was determined by the bottom gradients at bottom reflections between the source and the continental shelf. These characteristics are expected from a rough bathymetry as is encountered in that range.

C. EIGENRAY PROPAGATION LOSS ESTIMATION

Since it was not possible to fully calibrate the receiver system in order to determine the received pressure signal in pressure units the demodulated arrival time data contained only relative pressure squared amplitudes. To better identify the eigenray arrival times the procedure in Reference 11 was adapted to estimate the relative pressure squared values of the eigenrays (the eigenray with the least transmission loss was taken as the reference).

For two rays with similar characteristics (i.e. number of surface interactions and turning points) launched with a difference in elevation angle of $\Delta\theta$ the relative pressure squared, P^2_{rel}, can be given as

$$P^2_{rel} = \frac{\Delta\theta\cos\theta_0}{h\cos\theta}$$

(4.1)

where h is the vertical separation of the rays in meters at range r, θ_o is the original launch angle, θ is the angle at range r, and $\Delta\theta$ is the launch angular separation of the two rays. Figures 4.3 and 4.4 illustrate the geometries used to

31

measure these quantities, where the range R is one meter. This procedure gives a rough estimate only of the propagation loss along the raypath as it assumes azimuthal symmetry.
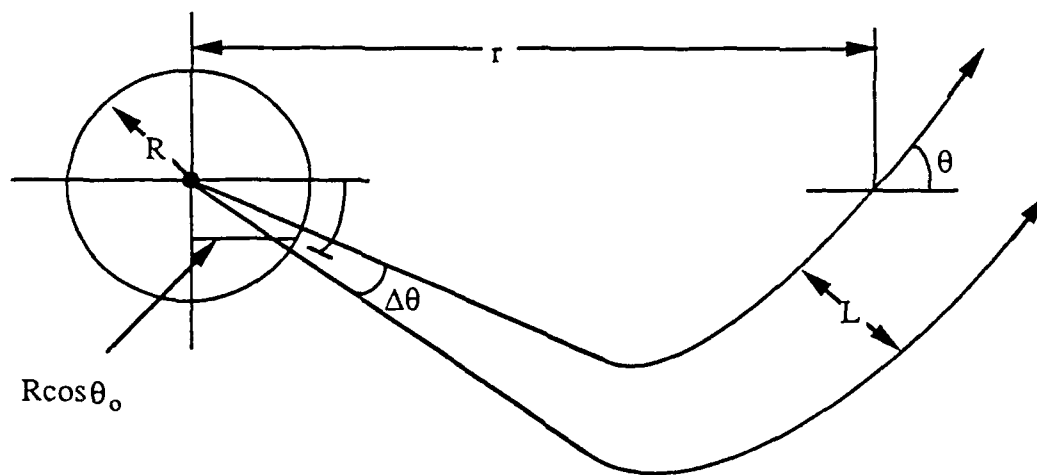

Figure 4.3. Spread of Power in a Horizontally Stratified Medium.
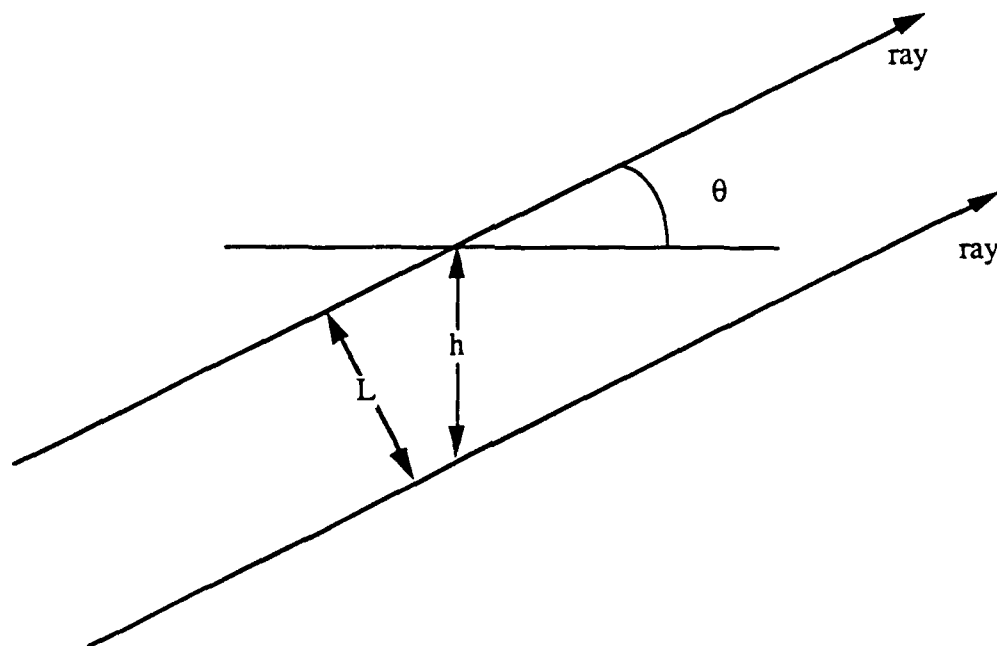

Figure 4.4. Geometry of Ray Separation.

Further this procedure neglects the effects of bottom interaction and does not quantify the bottom loss. To give a range of high and low expected transmission losses two cases were examined; no bottom losses and high bottom losses modeled by the interim Bottom Loss Upgrade values for 200 Hz. Figure 4.5 shows the bottom loss at 200 Hz as a function of grazing angle [Ref. 12].
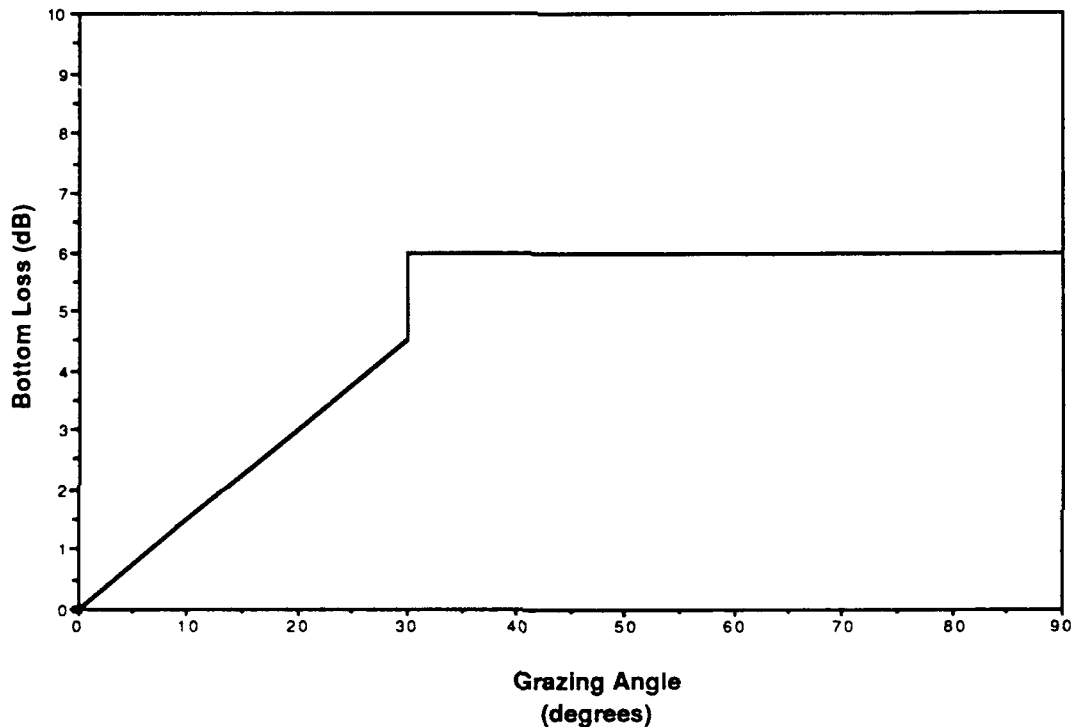
Figure 4.5. Interim Bottom Loss Upgrade Curve for 200 Hz.

D. EIGENRAY SENSITIVITY ANALYSIS

For the eigenrays found during the initial search it was important to quantify the sensitivity of each one to realistic changes in the environment. To do a sensitivity analysis there were two approaches that could be taken: a parametric approach or a phenomenalogical approach. The parametric approach requires

the ability to isolate a single parameter of the Hamiltonian equations of motion and to investigate the effects upon the raypath of perturbations in this parameter. The basic parameters for this model were: sound speed, bottom gradient and source/receiver positions. From the calculated eigenray paths it was found that changes to one of these parameters affected how the others were sampled by the raypath. For this reason the second approach, the phenomenalogical, was taken.

The phenomena modeled to determine the sensitivity of the eigenrays were: a two meter depth change simulating the tide within Monterey Bay; use of a second near surface sound speed profile (refer to Figure 3.4) and observations of the spacing of raypoints around the receiver position to investigate sensitivity of receiver position error.

The two meter tide was simulated by increasing the bottom depth by two meters while keeping the sound speed profile tied to the surface. This meant that the near surface sound speed profile would be unchanged and the sound speed at the bottom would be due to the increase in pressure due to the two meter increase in the water column height.

The change of sound speed profile was done by adding the second sound speed profile shown in Figure 3.4 to the deep sound speed profile and using CTANH to give the continuous version of this discrete profile. For this analysis the original bottom depths were used.

V. RESULTS AND CONCLUSIONS

A. RESULTS

A.1.   Initial Eigenrays

The initial search for eigenrays located six eigenrays with raypoints that were less than one half-wavelength from the specified receiver position. The launch angles, arrival time differences, the relative spreading loss (this is also the rigid bottom transmission loss), and the relative transmission loss (for a high loss bottom) for these six eigenrays are listed in Table 5.1.

Eigenray Identifier	Elevation angle (deg)	Azimuth angle (deg)	travel time difference, (milliseconds)	relative squared pressure including spreading loss	relative squared pressure including spreading loss and bottom loss
1	1.750980	20.472320	21.3	0.04	0.02
2	1.824000	20.441990	0.0	1.00	1.00
3	6.457500	20.421341	29.9	0.20	0.18
4	12.404990	19.668400	297.5	0.69	0.52
5	-3.602500	20.078520	565.2	0.44	0.00
6	12.800500	18.870410	568.2	0.01	0.08

Table 5.1.   Eigenray Launch Angles and Propagation Characteristics from Initial Identification Runs.

The arrival time differences indicate that the first three modeled arrivals would reach the receiver within the resolution width (62.5 milliseconds) of the

35

receiver and would therefore be unresolvable arrivals. The fourth arrival would be resolvable but the fifth and sixth modeled arrivals would also be unresolvable.

Figure 5.1 shows the vertical propagation of the combined raypaths (the individual raypaths can be found in Appendix A) and the bathymetry along each raypath as a function of range. The superposition of the bathymetry along each raypath shows that the eigenrays all travelled over the same bottom region and the two eigenray pairs with similar launch angles (1&2 and 4&6) travelled through the deep water with nearly identical raypaths. However, the characteristics of the shallow water propagation determined the travel time differences. Eigenray 2 had two more bottom bounces than eigenray 1 on the continental shelf and differed in travel time by only 21.3 milliseconds, while eigenray 6 had eight more bottom bounces but differed in travel time by 268 milliseconds. The significance of this difference in travel times is that for the receiver system used eigenray pair 1&2 would sample the same water but the results would be unresolvable after detection because the arrival time differences were less than the 62.5 millisecond receiver bandwidth. However the eigenray pair 4&6 is resolvable and the measured arrival time differences for this pair can give information about the dynamic water in the shallow region (the water mass where the two raypaths differ significantly).

Figure 5.2 shows a top view of the combined raypaths superimposed upon the bottom contours. It is evident from this figure that the bathymetry acted to filter the eigenrays so that the raypaths were close to the line-of-sight. Further any rays that deviated from the line-of-sight did not reach the receiver. For the computed eigenrays the maximum transverse distance from the line-of-sight was approximately 100 hundred meters.
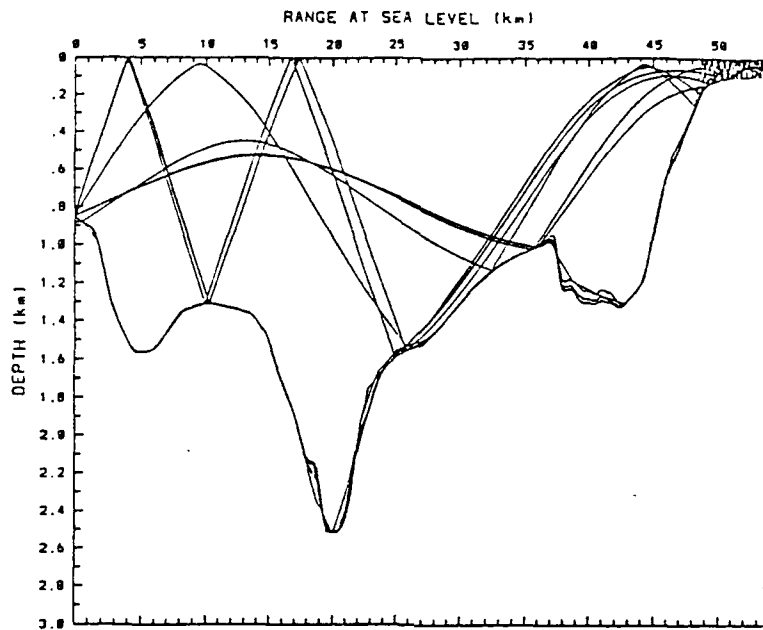
Figure 5.1. Combined Raypaths and Bathymetry for Initial
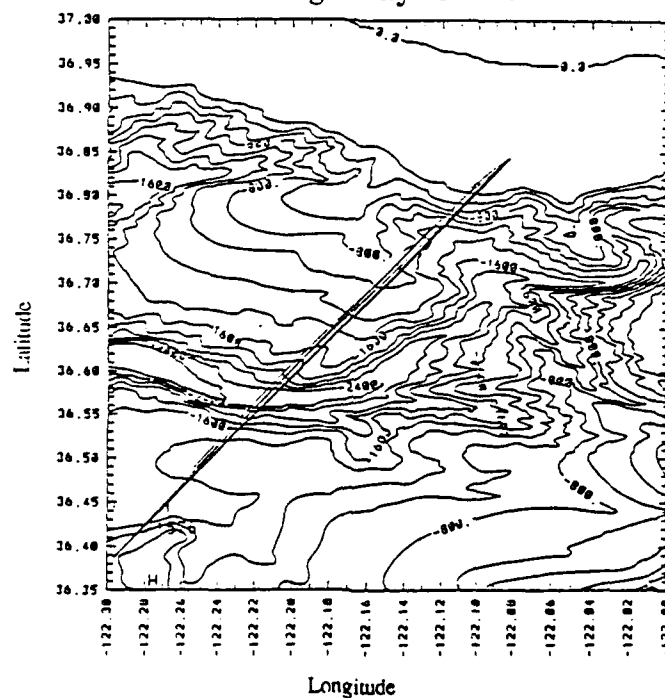Eigenray Search.

Figure 5.2 The Horizontal Paths of the Combined Eigenrays
Superimposed on 200 Meter Interval Bottom Contours.
The North-South and East-West Distances are not to the Same Scale.

Figure 5.3 is a stickplot of the arrival time differences and relative amplitudes for the six eigenrays. The reference eigenray was chosen as the one that had the least spreading and transmission loss, for this case it was also the first expected arrival. Comparison of the predicted arrival time differences with the resolution of the transmitted signal shows that:

1. There are three arrivals that arrive at the beginning of the expected arrival time sequence that are unresolvable (the arrival time spread is 29 milliseconds.

2. The second arrival time difference at 300 milliseconds is resolvable.

3. The third expected arrival period contains two arrivals spaced three milliseconds apart that are unresolvable.
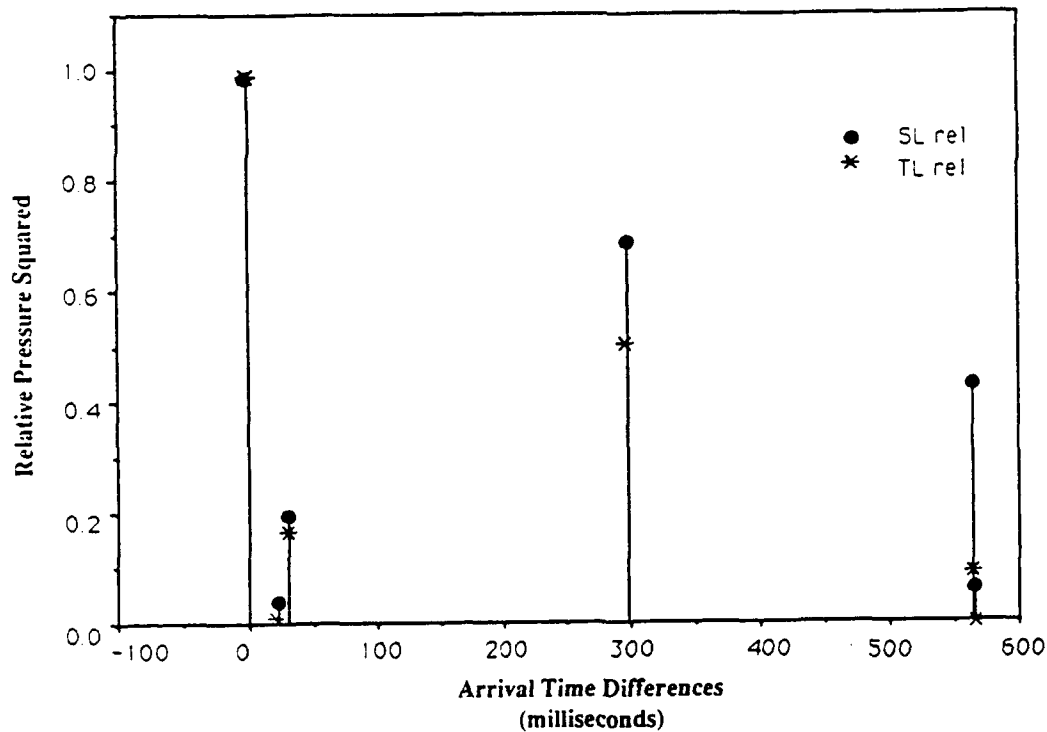
Figure 5.3. Arrival Time Differences versus Relative Squared Pressure with SpreadingLoss (SL rel) and Spreading and Bottom Loss (TL rel).

A.2. Eigenray Sensitivity Analysis.

Table 5.2 gives the results of the sensitivity analysis for the simulated tide of two meters. These eigenrays were found by searching in launch azimuth and elevation angles +/- 0.3° about the initially determined eigenray launch angles. The first observation is that the two arrivals with arrival time differences of 565 milliseconds were not found, for both cases opening the search window to +/- 1.0° did not lead to the relocation of any eigenrays.

Eigenray Identifier	Elevation angle (deg)	Azimuth angle (deg)	travel time difference, (milliseconds)	relative squared pressure including spreading loss	relative squared pressure including spreading loss and bottom loss
1	1.780000	20.475025	-40.5	0.77	0.93
2	1.781050	20.436001	36.9	1.00	0.28
3	6.466600	20.399000	0.0	0.93	1.00
4	12.702000	19.601500	314.5	0.35	0.11

Table 5.2.   Eigenray Launch Angles and Propagation
Characteristics from Tidal Sensitivity Analysis.

Figures 5.4 and 5.5 show the vertical and horizontal paths of the four eigenrays found in the tidal analysis. From Figure 5.4 it can be seen that the deep water paths of the four eigenrays relocated sampled the same deep water as the initial eigenrays with similar launch angles and had similar arrival time differences. Figure 5.5 indicates that the two eigenrays that were not relocated in this sensitivity analysis were the eigenrays with the maximum off line-of-sight deviation in the initial search. The individual raypaths illustrated in Appendix A

39

indicate that the shallow water propagation of eigenrays 2,3 and 4 had increased
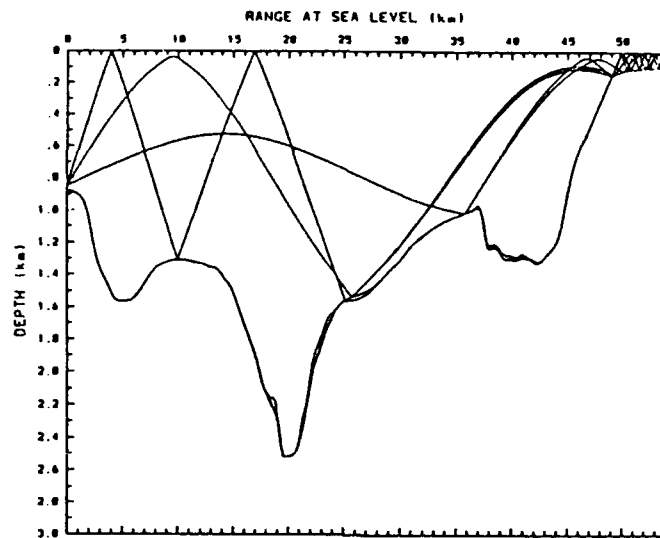number of bottom bounces.

Figure 5.4. Combined Raypaths and Bathymetry for Tidal
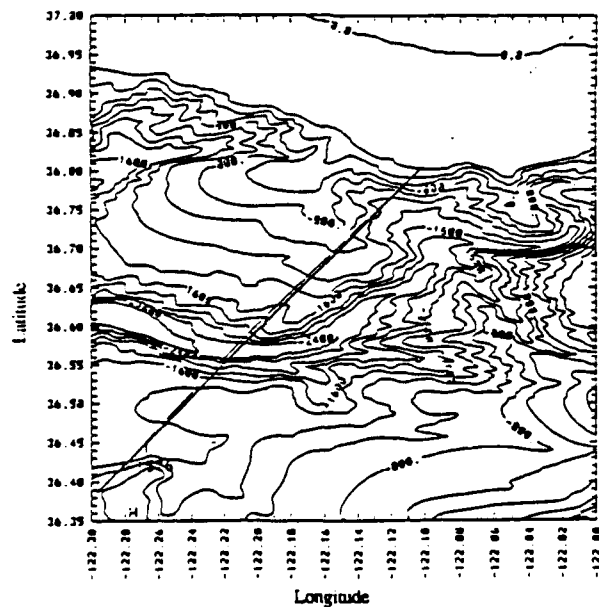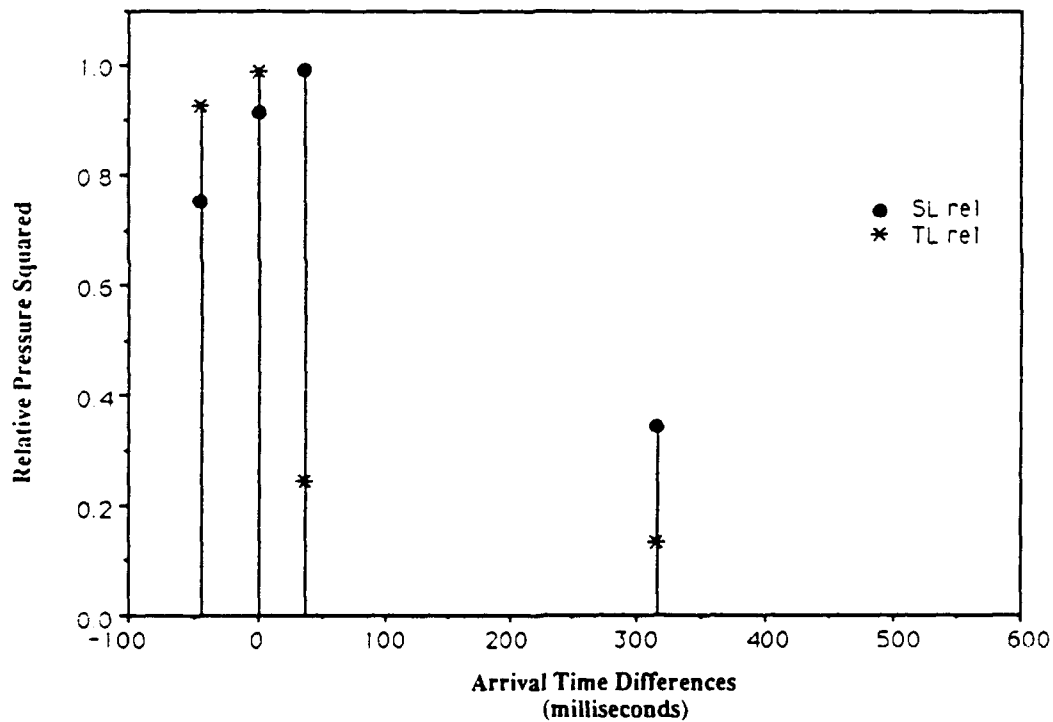Sensitivity Analysis.

Figure 5.5. The Horizontal Paths of the Combined Eigenrays
for the Tidal Sensitivity Analysis. The North-South and East-West
Distances are not to the Same Scale.

40

Figure 5.6 shows the stickplot of arrival time difference and relative propagation loss for the tidal sensitivity analysis eigenrays. This figure shows that:

1. The three first modeled arrivals are unresolvable.

2. The fourth arrival is resolvable and matches the eigenray path of eigenray 4 from the original search.

3. The two arrivals near 565 milliseconds in the initial search could not be relocated.

Figure 5.6. Arrival Time Differences versus Relative Squared Pressure with SpreadingLoss (SL rel) and Spreading and Bottom Loss (TL rel).

41

Table 5.3 shows the results of the sound speed sensitivity analysis. As has been discussed the sound speed profile used in this sensitivity analysis was measured at a significant distance from Station J and it is reasonable to assume that given the oceanographic conditions in Monterey Bay that it is a good estimate of the maximum change that could have occurred at Station J.

Eigenray Identifier	Elevation angle (deg)	Azimuth angle (deg)	travel time difference, (milliseconds)	relative squared pressure including spreading loss	relative squared pressure including spreading loss and bottom loss
1	1.820001	20.441989	-4.8	0.10	0.07
2	1.768499	20.414497	53.7	0.86	0.08
3	1.769000	20.472000	-50.0	0.29	0.33
4	6.464116	20.394617	0.0	1.00	1.00
5	12.702000	19.560995	-278.0	0.32	0.15

Table 5.3. Eigenray Launch Angles and Propagation Characteristics from Sound Speed Sensitivity Analysis.

As in the tidal sensitivity analysis the two initial search arrivals at 565 milliseconds were not relocated and all other original eigenrays were located. The travel time differences were found to be similar to both previous cases for the other modeled eigenrays and in this case three eigenrays were found with similar launch angles around $1.8°$ elevation and $20.4°$ azimuth as in the initial search (only two were located in the tidal sensitivity analysis search). Figure 5.7 shows that the same deep water was samples as in the initial and tidal searches

and Figure 5.8 shows that the horizontal deviation of the eigenray paths is similar to the tidal analysis.
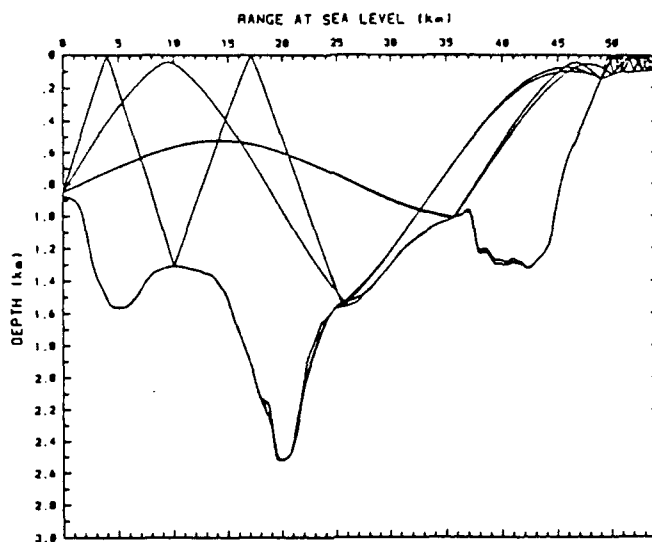

Figure 5.7. Combined Raypaths and Bathymetry for the Sound Speed Profile Sensitivity Analysis.
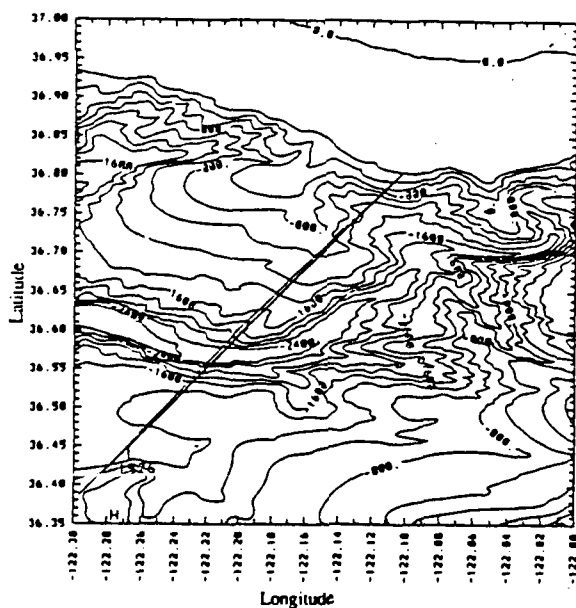

Figure 5.8. The Horizontal Paths of the Combined Eigenrays for the Sound Speed profile Sensitivity Analysis. The North-South and East-West Distances are not to the Same Scale.

Figure 5.9 shows the stickplot of arrival time difference and relative propagation loss for the sound speed profile sensitivity analysis eigenrays. This figure shows that:

1. The four first modeled arrivals are unresolvable.

2. The fifth arrival is resolvable and matches the eigenray path of eigenray 4 from the original search.

3. The two arrivals near 565 milliseconds in the initial search could not be relocated.
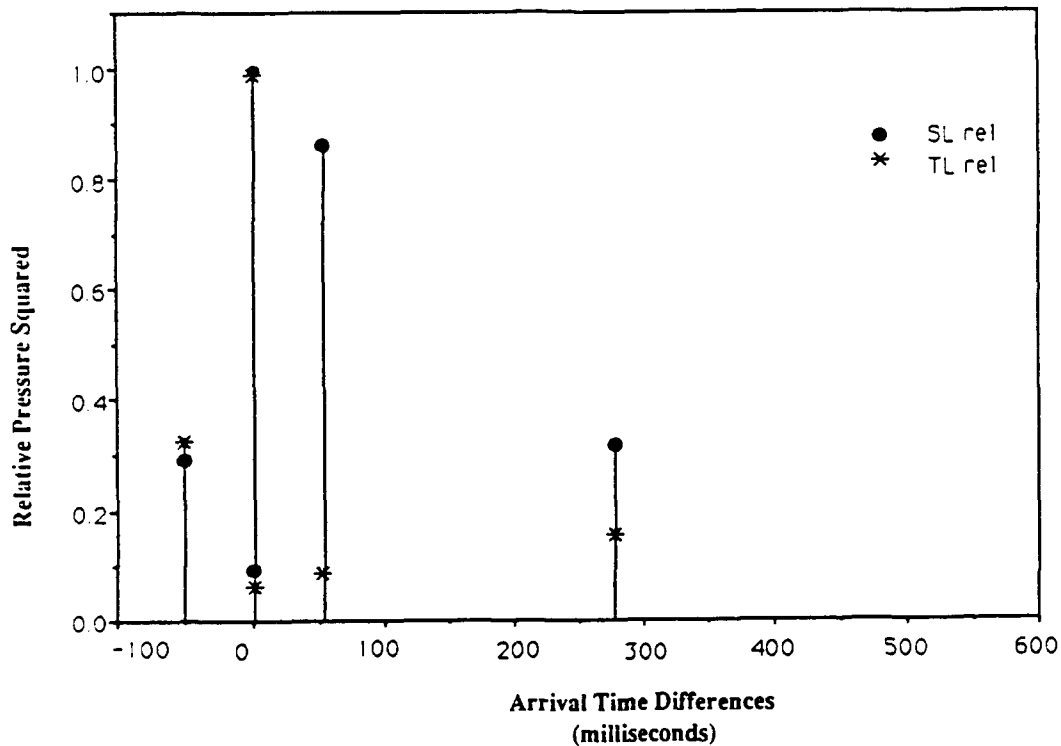
Figure 5.9. Arrival Time Differences versus Relative Squared Pressure with SpreadingLoss (SL rel) and Spreading and Bottom Loss (TL rel).

A.3. Comparison With Measured Arrival Times

Figure 5.10 shows a segment of the demodulated arrival sequences measured at Station J. The amplitudes are proportional to pressure squared and the horizontal axis is arrival time differences in seconds. Superimposed on this waterfall are three lines representing the arrival time differences modeled in the initial eigenray search at 0, 300, 565 milliseconds. These have been shifted to start at 1.25 seconds to match the measured arrivals.
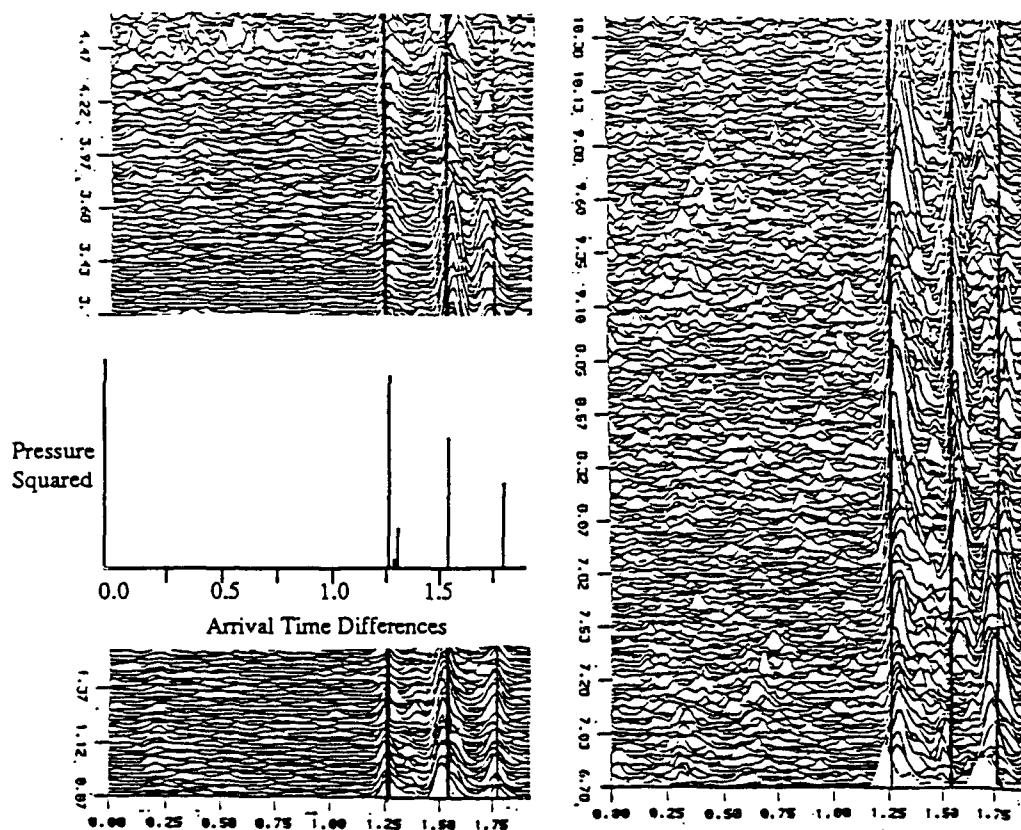
Figure 5.10. Segment of the Demodulated Tomographic Signal at Station J, 0045 to 1230 15DEC88. Inlay is the Stickplot of Eigenray Arrival Times and Amplitudes From the Initial Search.

45

These lines were placed by best lining up the modeled arrival time differences with the measured arrival time differences. By observing the behaviour of the signal arrivals with respect to these reference times it can be seen that:

1. The set of peaks (there are noticeably more than one) closest to the defined 0 arrival time reference (1.25 seconds on the time axis in Figure 5.10) vary in both strength and arrival time over short periods (in many cases over the 16 second averaging time) and that there are many double peaks. This would indicate multiple unresolved or partially resolved peaks that are also being smeared together by the averaging.

2. The signal arrival near the 300 milliseconds reference was visibly more stable, although it had a major dropout at 1.90 to 2.65 hours that corresponded to a dropout on the 0 and a decrease in the 565 millisecond arrival. This period is not shown in Figure 5.10.

3. The signal near the 565 millisecond reference varies in amplitude and time more than the arrivals around the 0 reference It also displays double peaks and characteristics similar to those expected of multiple arrivals. The results of the sensitivity analysis would suggest that this arrival should be more unstable. The possibility of an undetected eigenray at this time, which is suggested by the possibility of multiple arrivals, would account for its more stable structure.

The modeled arrival times for both the 0 and 565 millisecond references indicated unresolvable arrivals and the averaged data exhibits behaviour similar to this. However, the averaging technique used tends to hide the characteristics of the arrival signal. The unaveraged data indicates that some of the apparent double arrivals are due to single arrivals that shift in time over the averaging period. [Ref. 13]

The arrival time difference for the first two arrival groups using a non-linear tracker was found to be 265.2 +/- 42.0 milliseconds [Ref. 13]. The results of the initial eigenray search and sensitivity analysis show that the expected

46

arrival time difference for the strongest arrivals in these groups ranged from 278 to 314 milliseconds. This close agreement between the measured and modeled signal arrivals is a strong indication that the eigenrays modeled correspond to the actual eigenrays of the measured data.

The amplitude information suggests that the bottom loss in the shallow water region was low. This is best supported by the intermittent detection of the arrivals at 565 milliseconds. For a high loss bottom, as would be expected from the sediment types on the continental shelf, these arrivals were calculated to have negligible amplitude. To better determine the significance of the arrival amplitudes more information about the sediment structure would have to be incorporated in the bottom loss calculations.

B. CONCLUSIONS

The aim of this thesis was to model the acoustic propagation for the Monterey Bay Tomography Experiment. The results of the three-dimensional modeling of the acoustic propagation between the transmitter and Station J indicate:

1. The combination of a three-dimensional raytracing model, HARPO, and the environmental model of the Monterey Bay were successfully employed in matching the arrival time of three of the major arrivals measured at Station J.

2. The first rays launched in the initial eigenray search were along the line-of-sight between the transmitter and station J. None of these rays were found to be eigenrays. This indicates that the assumption of a zero bathymetry gradient in the azimuthal direction used to limit rays to two dimensions is inappropriate in modeling this complex bathymetry.

3. Although the raypaths of the eigenrays located exhibited very little horizontal deflection, the complex bathymetry was seen to have a major effect in preventing many rays from propagating onto the continental shelf or close

to Station J. This supports the requirement of a three-dimensional bathymetry input into a three-dimensional propagation model, such as HARPO, to accurately model the acoustic propagation in Monterey Bay.

4. There was visible variation of the signal arrival time and amplitudes in the measured data for the first (0 reference) arrival time and the 565 millisecond arrival time. This was explainable by the location of several eigenrays spaced less than the receiver resolution of 62.5 milliseconds at both these arrival times.

5. The detection of the arrivals at 565 milliseconds indicated that the bottom loss along this path lay between a high loss bottom (expected for the sediment on the continental shelf) and a perfect reflector.

6. Although the analysis of the received signals showed that there were insufficient resolvable eigenrays measured to use inverse techniques, there are indications that several improvements could be made to the experiment to improve reslovability of eigenrays. They are:

   a. Increase the bandwidth of the transmitted signal to increase the temporal resolution of the received signal.

   b. The range of elevation angles at the receiver for the modeled eigenrays was 3° to 24°. Use of a vertical array as a receiver would allow for exploitaion of this information via plane-wave beamforming and modal arrivals could be detected by mounting the receiver off of the bottom.

7. The incorporated environmental model, and in particular the 250 meter grid spacing of the bottom depths provided by NOAA, was sufficient to to enable the accurate determination of the eigenray paths for propagation over the complex bathymetry along the raypaths.
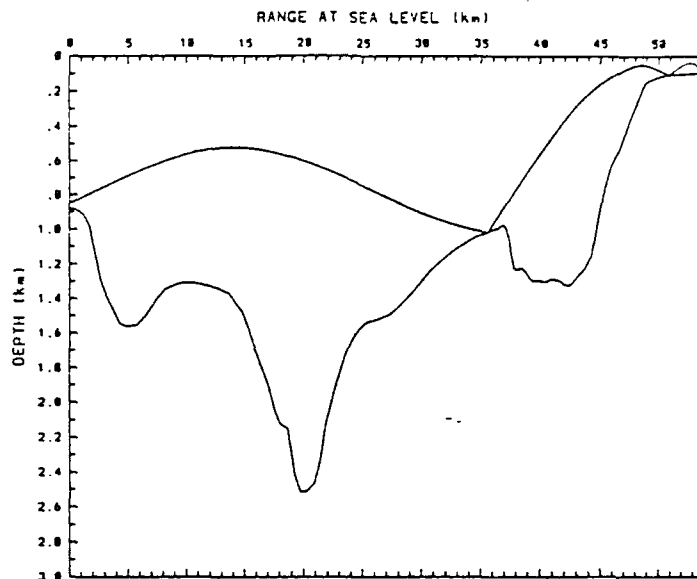
APPENDIX A

A. INITIAL EIGENRAYS

Figure A.1.   Eigenray 1
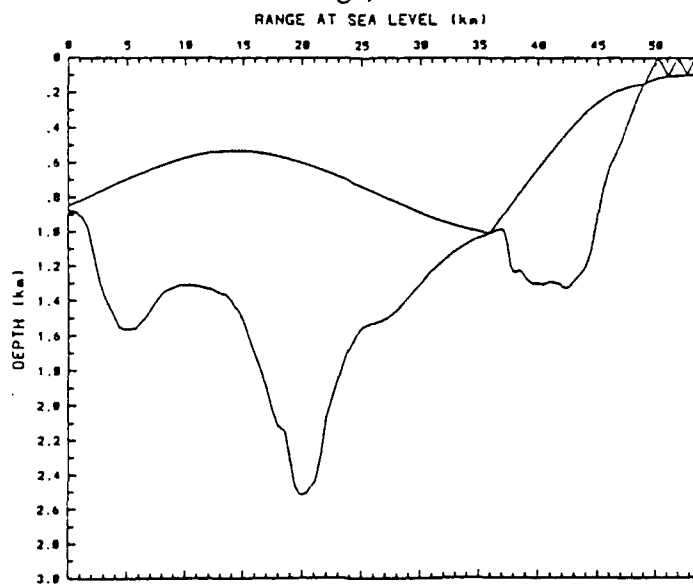Launch Azimuth = 20.472320 degs, Launch Elevation = 1.750980 degs.

Figure A.2.   Eigenray 2
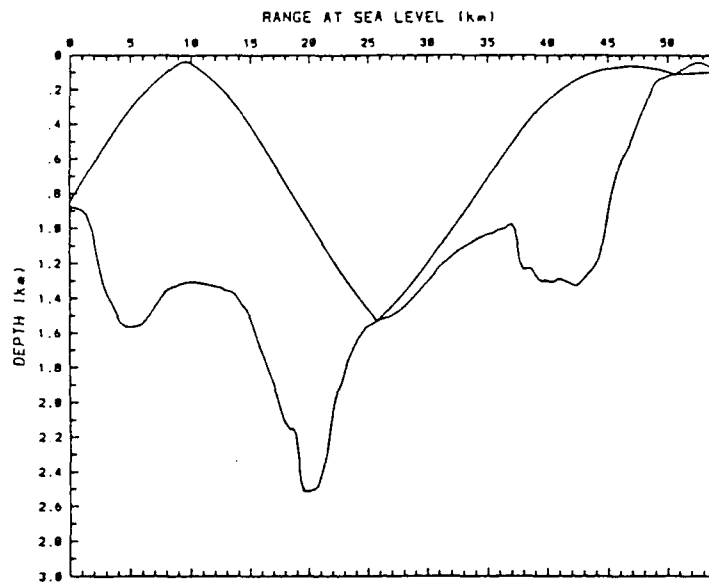Launch Azimuth = 20.442000 degs, Launch Elevation = 1.824000 degs.

Figure A.3. Eigenray 3
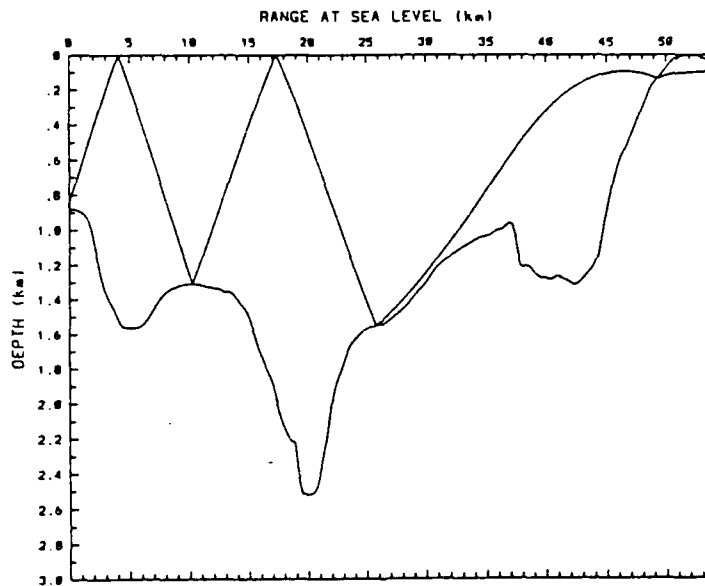Launch Azimuth = 20.421341 degs, Launch Elevation = 6.457500 degs.

Figure A.4. Eigenray 4
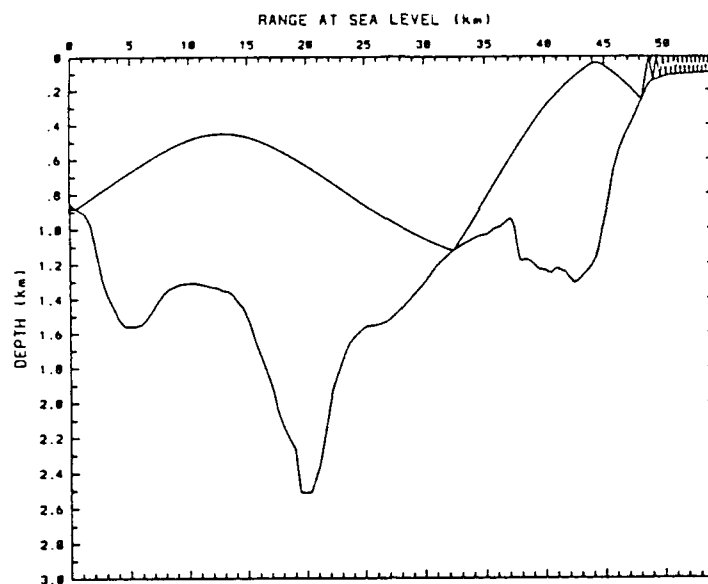Launch Azimuth = 19.668400 degs, Launch Elevation = 12.404990 degs.

50

Figure A.5.   Eigenray 5

Launch Azimuth = 20.078520 degs, Launch Elevation = -3.602500 degs.
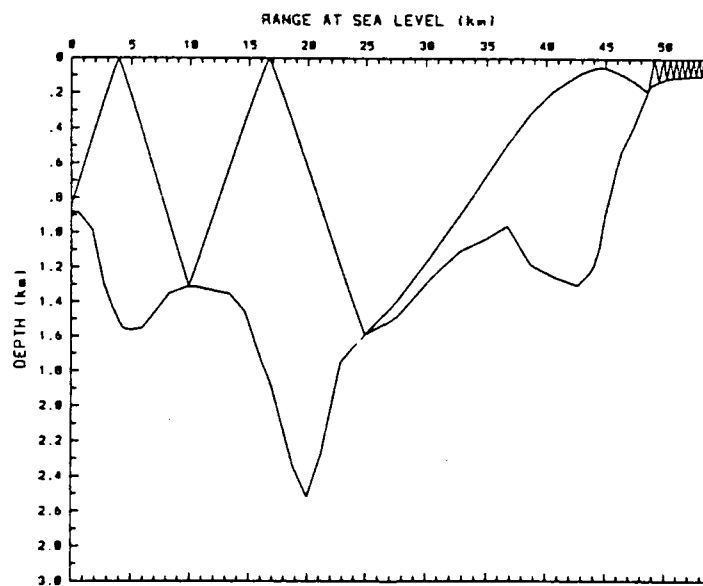
Figure A.6.   Eigenray 6

Launch Azimuth = 18.870410 degs, Launch Elevation = 12.800500 degs.

51

B. TIDAL SENSITIVITY ANALYSIS EIGENRAYS
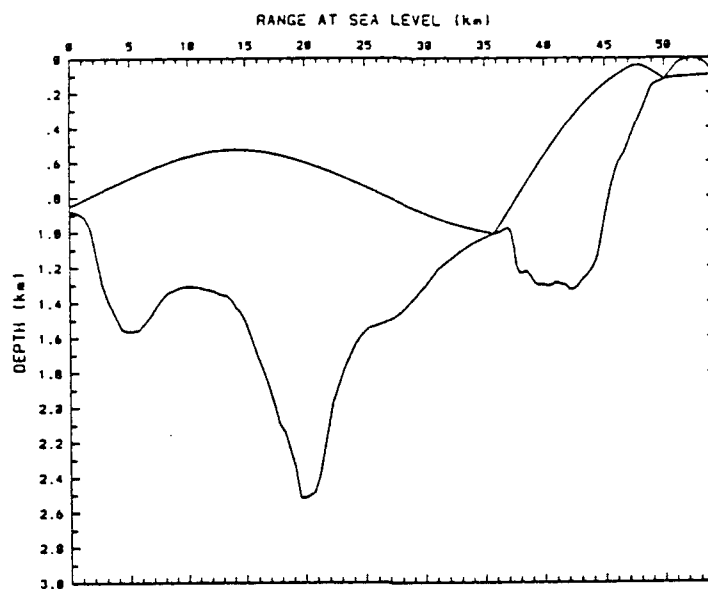
Figure A.7. Tidal Analysis Eigenray 1
Launch Azimuth = 20.475025 degs, Launch Elevation = 1.780000 degs.
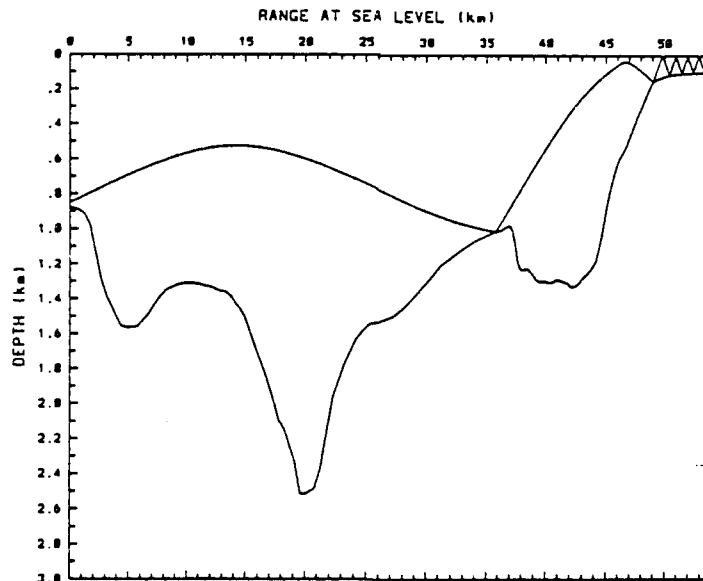
Figure A.8. Tidal Analysis Eigenray 2
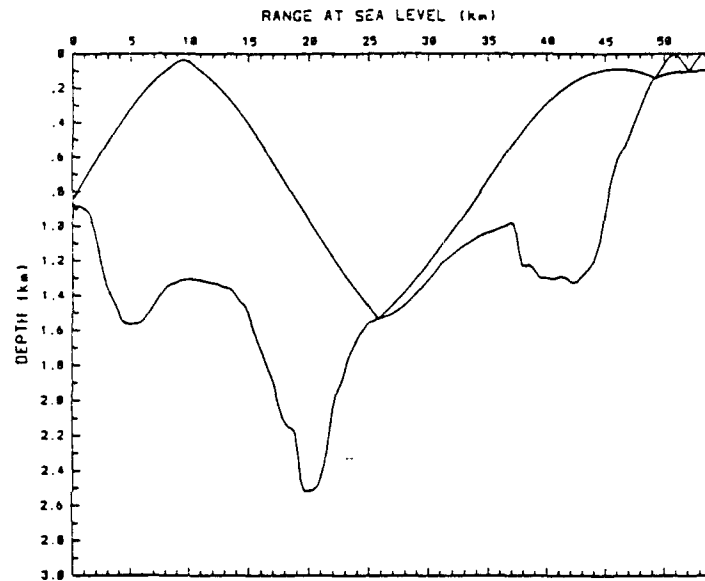Launch Azimuth = 20.436001 degs, Launch Elevation = 1.781050 degs.

Figure A.9. Tidal Analysis Eigenray 3
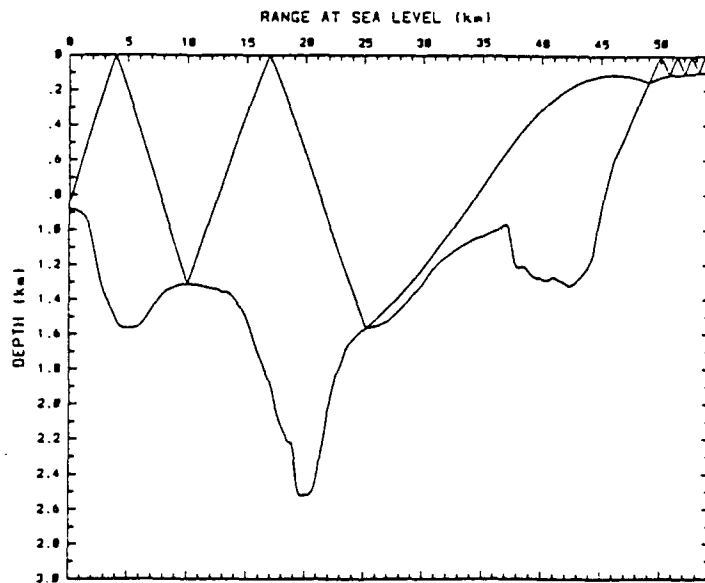Launch Azimuth = 20.399000 degs, Launch Elevation = 6.466600 degs.

Figure A.10. Tidal Analysis Eigenray 4
Launch Azimuth = 19.601500 degs, Launch Elevation = 12.702000 degs.

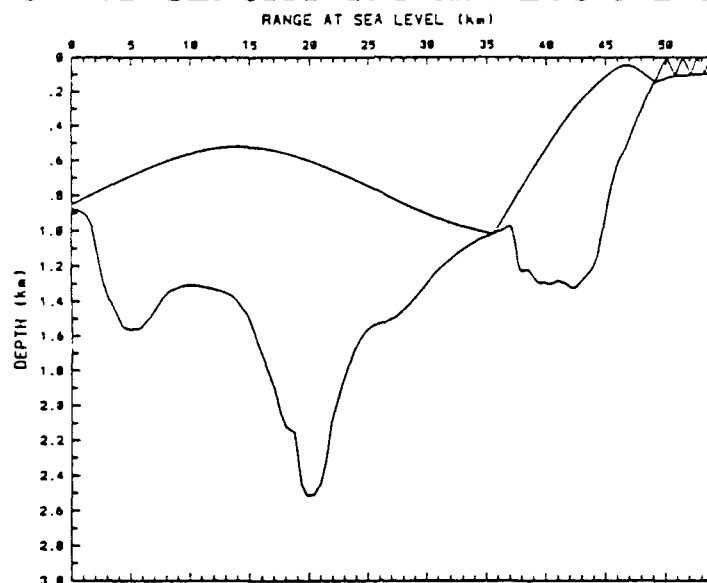# C. SOUND SPEED SENSITIVITY ANALYSIS EIGENRAYS

RANGE AT SEA LEVEL (km)

Figure A.11. Sound Speed Analysis Eigenray 1

Launch Azimuth = 20.441989 degs, Launch Elevation = 1.820001 degs.
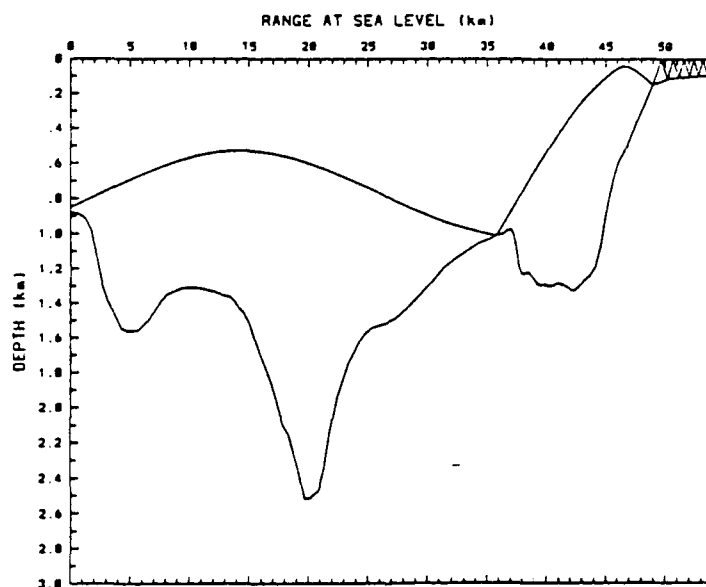
RANGE AT SEA LEVEL (km)

Figure A.12. Sound Speed Analysis Eigenray 2

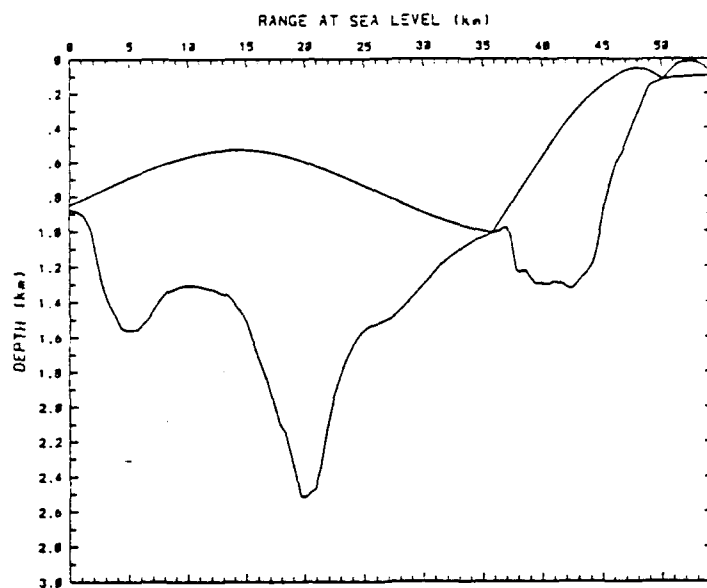Launch Azimuth = 20.414497 degs, Launch Elevation = 1.768499 degs.

54

Figure A.13. Sound Speed Analysis Eigenray 3

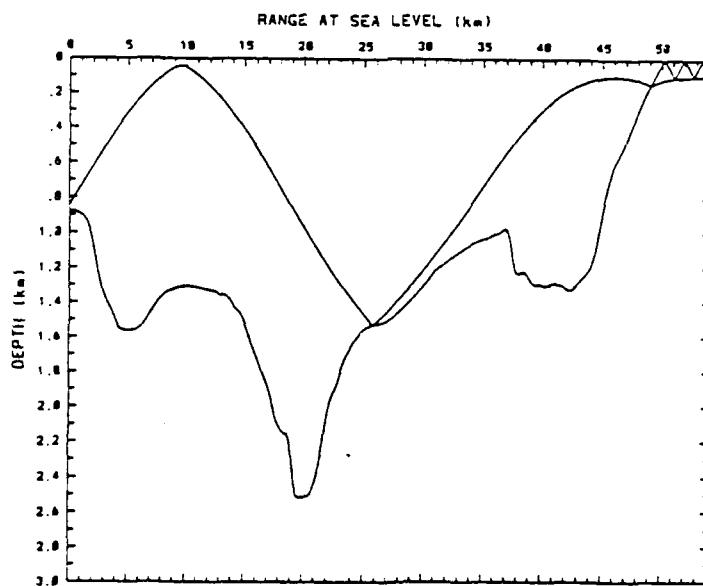Launch Azimuth = 20.472000 degs, Launch Elevation = 1.769000 degs.

Figure A.14. Sound Speed Analysis Eigenray 4

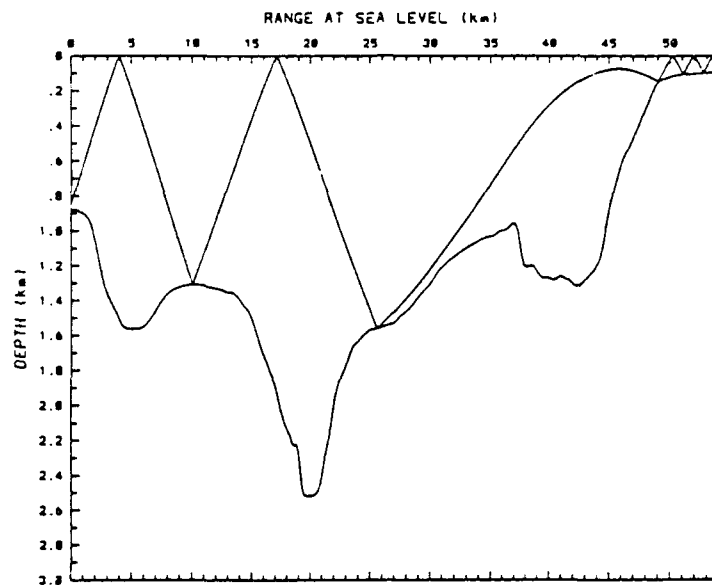Launch Azimuth = 20.394617 degs, Launch Elevation = 6.464116 degs.

Figure A.15. Sound Speed Analysis Eigenray 5
Launch Azimuth = 19.560995 degs, Launch Elevation = 12.702000 degs.

References

1. Spindel, R.C., "Ocean Acoustic Tomography: A Review,"*Current Practices and New Technology in Ocean Engineering*, volume 11, pp. 7 - 13, 1986.

2. Dees, Robert C., *Signal Processing and Preliminary Results in the 1988 Monterey Bay Tomography Experiment*, MS Thesis, Naval Postgraduate School, Monterey, CA, June 1989.

3. Jones, R.M., Riley, J.P., and Georges, T.M., *HARPO. A Versatile Three-Dimensional Hamiltonian Ray-tracing Program for Acoustic Waves in an Ocean with Irregular Bathymetry*, pp 1 - 252, Wave Propagation Laboratory NOAA, Boulder, Colorado, 1986.

4. Ugincius, Peter, "Ray Acoustics and Fermat's Principle in a Moving Inhomogeneous Medium," *The Journal of the Acoustical Society of America*, volume 5, number 5 (part 2), pp. 1759 - 1765, 1972.

5. Lighthill, James, *Waves in Fluids*, pp. 318 - 320, Cambridge University Press, 1978.

6. Rowan, Theresa M., *Monterey Bay Acoustic Tomography: Ray Tracing and Environmental Assessment*, MS Thesis, Naval Postgraduate School, Monterey, CA, September 1988.

7. National Oceanic and Atmospheric Administration, *Documentation for Dissemination of NOS/NOAA Gridded EEZ Bathymetric Data*, Ocean Mapping Section, N/CG224, NOAA Rockville Maryland.

8. Kao, Chih-Chung, *A Study of the Sensitivity of the Greenland Sea Acoustic Tomography Array*, pp. 21 - 23, MS Thesis, Naval Postgraduate School, Monterey, CA, December 1989.

9. Mercer, J.A., Felton, W.J., and Booker, J.R.,"Three-dimensional Eigenrays Through Ocean Mesoscale Structure," *The Journal of the Acoustical Society of America*, volume 78, number 6 , pp. 157 -163, 1985.

10. Personal Communication between J.H. Miller and R. M. Jones, September 19, 1990.

11. Clay, Clarence S. and Medwin, Herman, *Acoustical Oceanography*, pp. 91 - 93, John Wiley & Sons, 1977.

12. Interim Bottom Loss Upgrade Curve implemented in the Naval Postgraduate School Raytrace code.

13. Chaulk, Edwin K., *Arrival Time Tracking of Partially Resolved Acoustic Rays with Application to Ocean Acoustic Tomography*, MS Thesis, Naval Postgraduate School, Monterey, CA, December 1990.

INITIAL DISTRIBUTION LIST

No. Copies

1. Defense Technical Information Center   2
   Cameron Station
   Alexandria, VA 22304-6145

2. Library, Code 52   2
   Naval Postgraduate School
   Monterey, CA 93943-5002

3. Prof. James H. Miller, Code EC/Mr   5
   Department of Electrical and Computer Engineering
   Naval Postgraduate School
   Monterey, CA 93943

4. Prof. Ching-Sang Chiu, Code OC/Ci   1
   Department of Oceanography
   Naval Postgraduate School
   Monterey, CA 93943

5. Prof. Curtis A. Collins, Code OC/Co   1
   Department of Oceanography
   Naval Postgraduate School
   Monterey, CA 93943

6. Dr. James F. Lynch   1
   Woods Hole Oceanographic Institute
   Woods Hole, MA 02543

7. Lt(N) Donald F. Smith   2
   National Defence Headquarters
   101 Colonel By Drive
   Ottawa, Ontario
   K1A 0K2
   Canada
   Attn: DMCS-3 (St. Laurent Building)

8. Dr. Mark McIntyre   1
   Defence Research Establishment Atlantic
   9 Grove Street
   PO Box 1012
   Dartmouth, Nova Scotia
   B2Y 3Z7
   Canada